Vibrational Relaxation of N_2 Isolated in an Argon Matrix

Thesis by

Thomas Edward Orlowski

In Partial Fulfillment of the Requirements for the Degreee of

Master of Science

California Institute of Technology

Pasadena, CA 91125

1976

(Submitted August 29, 1975)

I. Acknowledgments

This thesis is dedicated to Chris whose patience, encouragement, and confidence made long hours of experiments and preparation worthwhile, and to my parents whose countless sacrifices made my entire education possible.

I would like to thank my advisor, G. Wilse Robinson, for fostering a new degree of independence in me. Special thanks should also go to the members of our group, and especially Jackie Berg, for helpful discussions throughout the course of the research.

I would also like to acknowledge the shops of the Chemistry department and Mr. William Schuelke for his help in the design of many components crucial to the apparatus.

II. Abstract

The Raman spectrum of N_2 isolated in an argon matrix at 4.2°K was obtained using single photon counting techniques and a CW argon ion laser. Attempts at measuring the vibrational relaxation (VR) time for N_2 were made by monitoring the Raman intensity from upper vibrational levels as a function of time. Stimulating the Raman process using a rhodamine 6G jet stream dye laser tuned to the Stoke's frequency while simultaneously irradiating with the argon ion laser, was also attempted in an effort to improve Raman intensity. Although an accurate measurement of the VR time awaits a more efficient excitation process (or a more powerful laser), our results indicate a VR time as long as a few minutes is possible for N_2 in this environment.

Table of Contents

III. Introduction

The study of energy transfer processes of small molecules isolated in rare gas matrices has received a great deal of experimental and theoretical attention in the recent past. Using a frequency doubled CO_2-N_2-He laser, Dubost et al.[1] measured a rather long fluorescence life time (4 msec) for 1% CO $X(^1\Sigma^+)$ in an argon matrix. Allamandola and Nibler[2] found a vibrational relaxation time of 1.2 msec for 0.05% C_2^- $(^2\Sigma_g^+)$ in an argon matrix upon excitation with a tunable Rhodamine-6G dye laser. Both of these experiments indicate that vibrational relaxation (VR) can indeed be slow in the proper environment.

Tinti and Robinson,[3] in an earlier experiment, found a vibrational relaxation time for N_2 in the $A(^3\Sigma_u^+)$ state on the order of 1 sec using X-ray excitation of a N_2 doped (1%) argon matrix. This extremely long VR time prompted the investigation that is the subject of this report.

In its ground $X(^1\Sigma_g^+)$ state, N_2 has a substantially larger vibrational energy spacing (2331 cm^{-1}) than in its $A(^3\Sigma_u^+)$ state (1460 cm^{-1}). Recent theoretical studies[4-7] (and foresight by Tinti and Robinson) suggest that N_2 $X(^1\Sigma_g^+)$ should therefore have a much longer VR time when isolated in a rare gas matrix invoking an inefficient multiphonon process as the most likely relaxation mechanism. The object of our experiments will be to measure the vibrational relaxation time of N_2 $X(^1\Sigma_g^+)$ in this environment and to determine the effect of temperature, concentration, rare gas host, and isotope substitution.

IV. Experimental

The experiments described herein involve matrix isolation techniques[8] and the use of a CW argon ion laser and rhodamine 6G jet stream dye laser to vibrationally excite the N_2 molecules in a Raman scattering process.

Experiments completed to date employed Matheson research grade argon (99.9995%) and nitrogen (99.9995%). Both gases are used without further purification. Mixtures of N_2 and Ar are prepared in a glass vacuum line using a continuous flow technique. Before mixing the gases, the vacuum manifold is evacuated to a pressure of 1×10^{-5} torr using a CVC 2" diffusion pump appropriately baffled to minimize contamination by pump oil. Gas flow rates are controlled by calibrated Granville-Phillips variable leaks set such that the ratio of flow rates (argon/nitrogen) is approximately 130. This produces a matrix containing 0.8% N_2. The rate of deposit was varied from 15 to 50 mmoles/hr and deposit times of up to 23 hours were employed.

The gas mixture enters a rotatable dewar through a nozzle which injects it upon a chromium plated copper target attached to a liquid helium cryostat. The target is hollow and in direct contact with coolant. Attached to its bottom is a silicon diode for temperature measurement. Surrounding the target is a copper heat shield in thermal contact (via indium seal) with the liquid N_2 reservoir surrounding the liquid helium cryostat. The heat shield is constructed with saphire windows (indium sealed) at 90° to each other such that the incident laser light can enter and the scattered Raman light can be collected as shown in Figure 1.

Figure 1. Top view of cryostat base

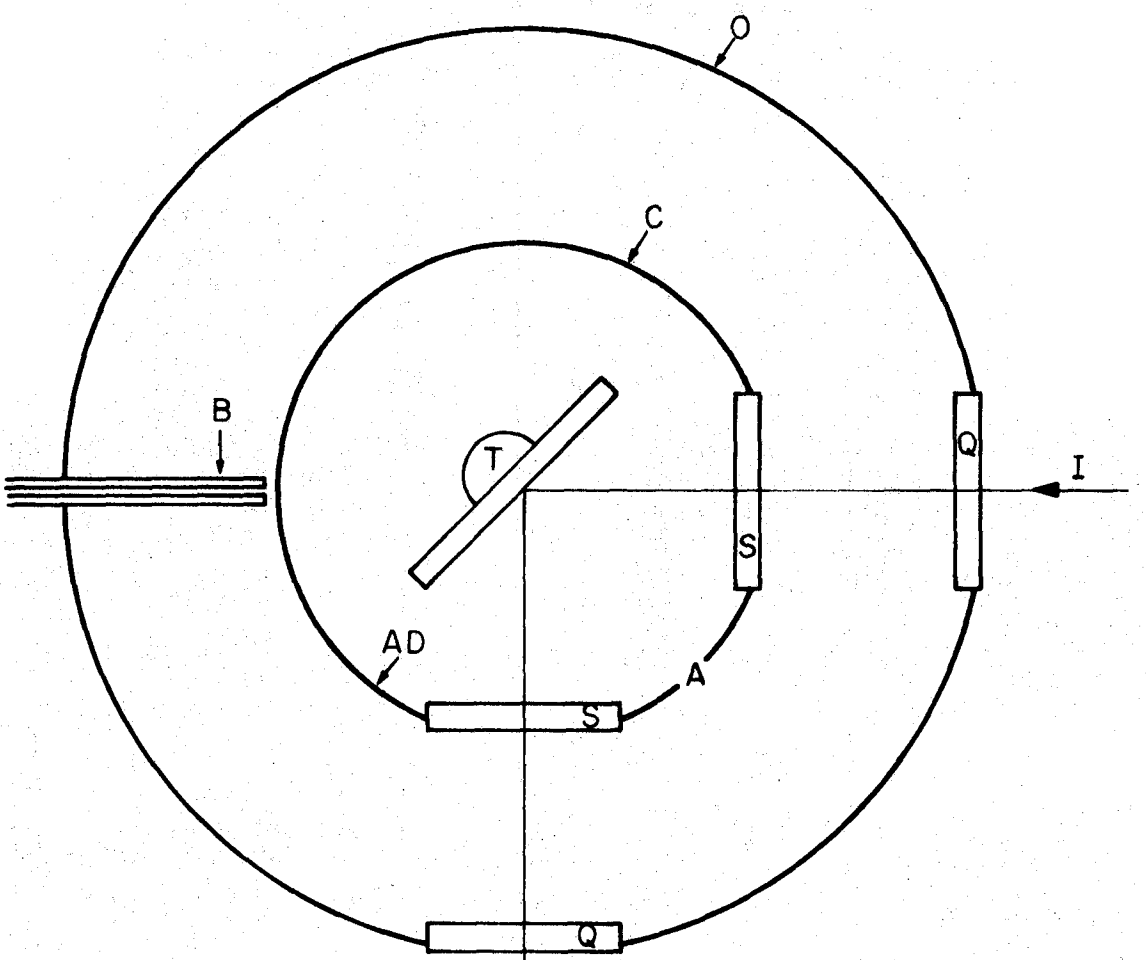

I - incident laser beam
R - Raman scattered light
AD - inside of heat shield is coated with aquadab to absorb scattered incident light
Q - quartz window
S - saphire window
O - outside wall of dewar
C - copper heat shield
T - chrome plated target attached to helium dewar
A - gas inlet
B - gas nozzle

Note: Dewar is rotated such that A aligns with B for depositing.

Attached to the cryostat base is a gate valve separating the dewar assembly from a Freon-baffled 4" CVC diffusion pump. While the deposit is being made, this gate valve can be closed allowing the deposit to form and anneal rapidly or left open giving a more crystalline deposit. After the deposit is formed, the gate valve is opened and during experiments pressure inside the matrix chamber is $<1 \times 10^{-7}$ torr due to efficient cryo-pumping by the liquid helium.

Vibrational excitation of nitrogen in the matrix is accomplished using a Spectra Physics Model 170 argon ion CW laser. With a prism for tuning in the rear reflector assembly, we are able to realize a maximum output power (TEM_{00}) of 5.6 watts at 4879.9 Å with 40 amps at 550v DC supplied to the discharge tube. The laser is mounted on a NRC vibration isolation optical table. Light scattered from the matrix is collected with a quartz lens and after removing unwanted laser light at the incident frequency using Valpey or CVI dielectric coatings, it enters a Jarrel-Ash Model 78-400 1.83 meter scanning spectrometer. This spectrometer has an effective aperature ratio of F/11.6 and a first order reciprocal linear dispersion of 9.0 Å/mm. We use a slit width of 55 microns for a resolution of 0.5 Å.

In all our experiments, data is gathered and processed using single photon counting techniques.[9] First, light is detected at the exit slit of the spectrometer by an EMI 6256S high gain photomultiplier (PMT). It is housed in a Products for Research RF shielded, dry-ice cooled, photomultiplier housing. The PMT is supplied with -2500 volts by a Keithley Model 246 high voltage power supply.

A special cable was constructed with double shielding to carry the

photomultiplier signals. The cable is terminated at 50 ohms and care was taken to eliminate all ground loops. PMT signals are received by an EG and G counting module. There they are amplified 64 times by AN 101 broadband linear amplifiers before passing into a TR 104S discriminator whose threshold is set to maximize signal to noise. The scalar output of the discriminator is fed into a Nuclear Data series 2200 multichannel analyzer (MCA).

With this type of signal processing, single photon pulses from the PMT show up as counts in channels of the analyzer. During an experiment, the spectrometer slowly scans (0.25 Å/min) and the MCA advances channels automatically at predetermined time intervals. Syncronization was accomplished using a digital clock interface. Soon after the spectrometer begins scanning, a microswitch is closed which starts the clock. It sends a start pulse to the MCA which then "opens" the first channel. At the end of a predetermined time interval (2 minutes in our case), the clock records the channel number in a LED display and sends another pulse to the MCA causing it to advance to the next channel. In this manner, a spectrum can slowly be obtained.

Data (counts/channel) from the MCA is displayed on a Tektronix Model 547 oscilloscope. Plots of the spectrum are obtained using a Hewlett Packard Model 7590 C point plotter interfaced with the MCA, and a teletype 33-KSR printer is available for permanent data storage on punched paper tape.

After a matrix has been deposited on the target, a careful alignment procedure is followed to maximize the photon gathering power of our

detection system. The laser beam is focused on the target using a 25 mm FL quartz lens. Scattered light is collected by a 50 mm FL quartz lens, collimated and refocused at the entrance slit of the spectrometer by a 100 mm FL quartz lens. For alignment purposes only, a chopper is placed along the optical axis and the PMT is connected to a PAR HR-8 lock-in amplifier. Lens positions are varied using translation stages until a maximum signal from the laser (attenuated by neutral density filters) registers on the PAR. We have found that very small adjustments in the alignment have improved signal strength two to four orders of magnitude! Figure 2 shows the experimental set-up for initial results described in the following section.

Figure 2. Schematic diagram of the experimental set-up

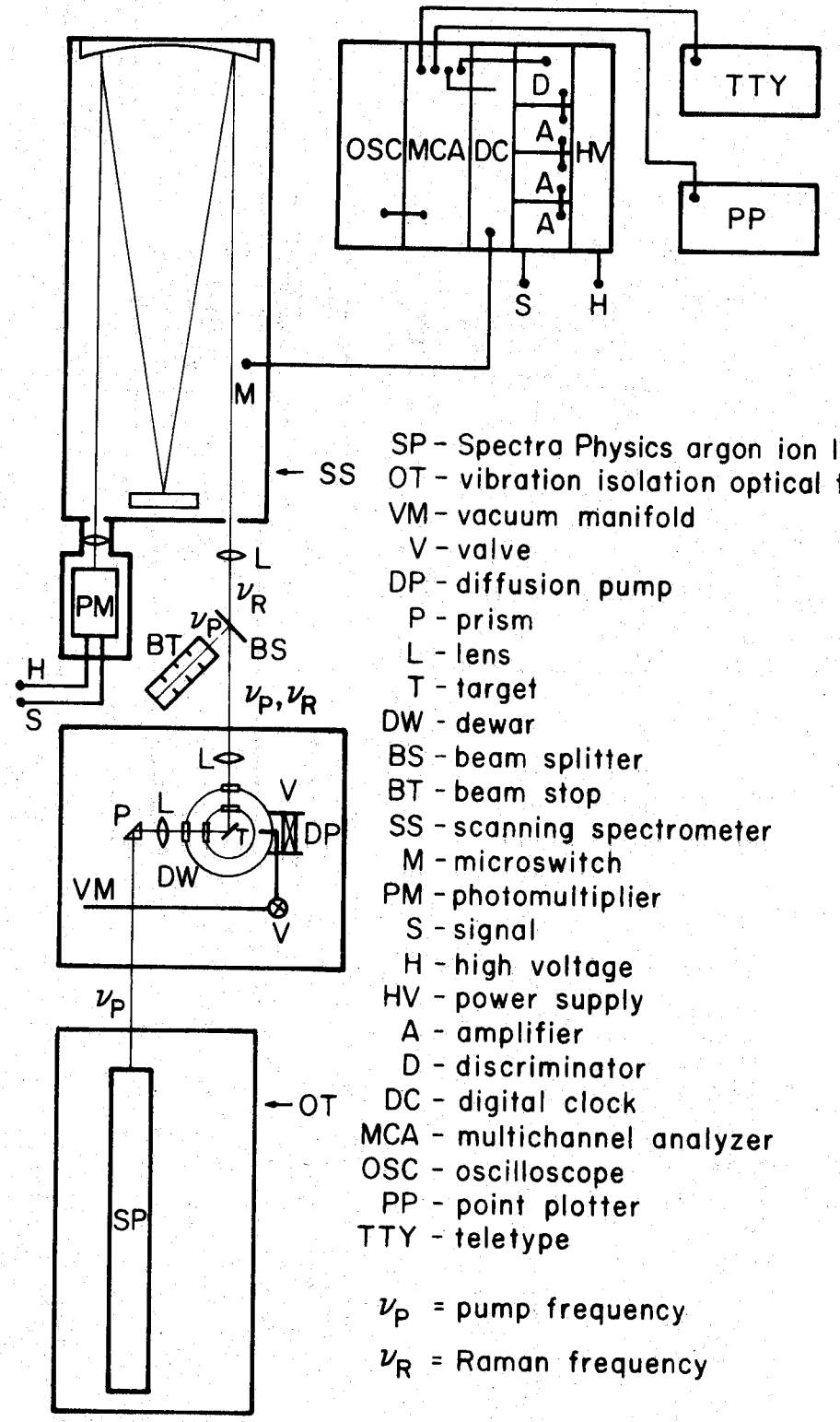

SP - Spectra Physics argon ion laser
OT - vibration isolation optical table
VM - vacuum manifold
V - valve
DP - diffusion pump
P - prism
L - lens
T - target
DW - dewar
BS - beam splitter
BT - beam stop
SS - scanning spectrometer
M - microswitch
PM - photomultiplier
S - signal
H - high voltage
HV - power supply
A - amplifier
D - discriminator
DC - digital clock
MCA - multichannel analyzer
OSC - oscilloscope
PP - point plotter
TTY - teletype

ν_P = pump frequency

ν_R = Raman frequency

V. Experimental Results

Upon excitation of an N_2 doped argon matrix with 5.0 watts at ν_L=4879.9 Å and scanning through the Raman Stoke's region for N_2 at 0.25 Å/min, we were able to obtain the spectrum shown in Figure 3. A log scale was used so that all channels could be displayed on the same plot without losing detail in the spectrum. Each channel was open for two minutes and thus contains 0.5 Å of spectral information.

Raman transitions should occur following the selection rule:[10] $\Delta\nu=\pm1$. Therefore, the Raman spectrum of an anharmonic oscillator should contain lines shifted from the exciting line by an amount corresponding to the vibration frequency with spacings determined by the anharmonicity of the oscillator. The number of lines one sees depends upon the population of the upper vibrational levels. Term values for the $X(^1\Sigma_g^+)$ state of N_2 can be calculated following Herzberg's notation[11]

$$G(\nu) = \omega_e(\nu + \tfrac{1}{2}) - \omega_e x_e(\nu + \tfrac{1}{2})^2 + \omega_e y_e(\nu + \tfrac{1}{2})^3$$

Vibrational constants, term values, and vibrational spacings $\{\Delta G(\nu) = G(\nu+1) - G(\nu)\}$ for the X state of N_2 are found in Table I. From this table one can see that the anharmonicity ($\Delta\Delta G(\nu)$) in the stretching vibration of N_2 is approximately 29 cm^{-1}. Table II shows the wavelength (λ_R) and frequency (ν_R) of the observed Raman Stoke's lines, the N_2 stretching frequency ($\nu_s = \nu_L - \nu_R$), vibrational spacings $\Delta G(\nu)$ from Table I, and the tentative assignments. Reported frequencies are accurate to approximately ±2 cm^{-1}.

Figure 3. Raman spectrum for N_2 doped argon matrix at 4.2°K

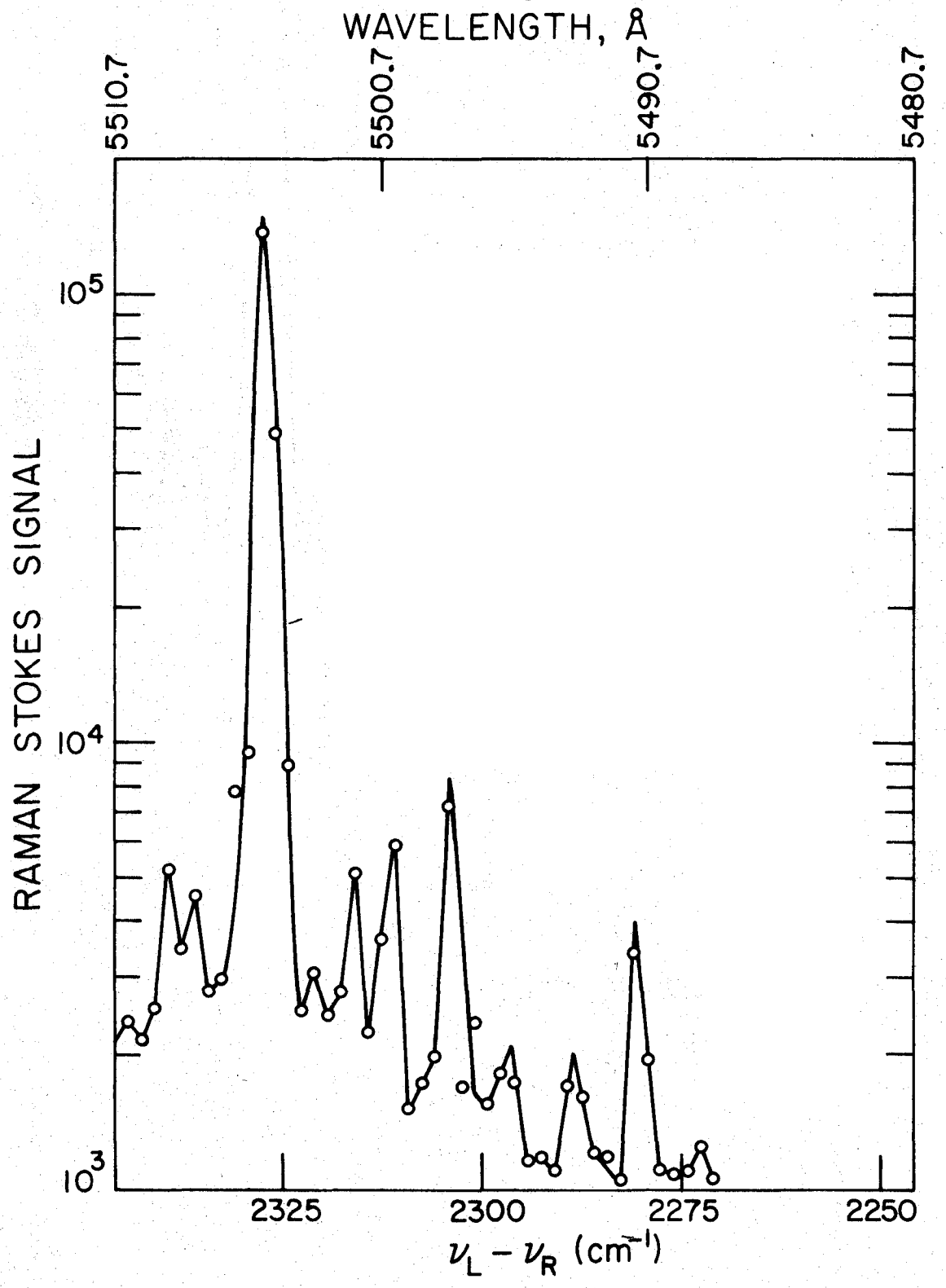

Table I. Molecule Constants of N_2

Vibrational constants	(cm^{-1})[11]
ω_e	2359.6
$\omega_e x_e$	14.456
$\omega_e y_e$	0.00751
Term values	
G(0)	1176.2
G(1)	3506.9
G(2)	5808.8
G(3)	8081.9
Vibrational spacings	
$\Delta G(0)$	2330.7
$\Delta G(1)$	2301.9
$\Delta G(2)$	2273.1

Table II. Raman Stoke's Lines for N_2 Doped Argon Matrix

λ_R(Å)	$\nu_R(cm^{-1})$	$\nu_L-\nu_R(cm^{-1})$	$\Delta G(\nu)$	Assignment
5505.2	18164.6	2327.2	2330.7	$\nu_s(1\leftarrow 0)$
5501.7	18176.2	2315.6		
5500.2	18181.2	2310.6		
5498.0	18188.4	2303.4	2301.9	$\nu_s(2\leftarrow 1)$
5496.0	18195.1	2296.8		
5493.5	18203.3	2288.5	2290.7[12]	$\nu_s(^{15}N\text{-}^{14}N)(1\leftarrow 0)$
5490.9	18212.0	2279.8	2273.1	$\nu_s(3\leftarrow 2)$

The unassigned lines are difficult to account for unambiguously.[31,32] The weak lines on the red side of the large ν=0 line are seen in a blank (no matrix) scan over the same region. The other unidentified lines may appear (too weak to say) in the blank spectrum which was obtained at lower laser power or they could result from combinations of ν_s plus lattice modes ν_ℓ. Weak lines in the Raman spectrum of solid $N_2(\alpha\text{-}N_2)$ attributed to $(\nu_s+\nu_\ell)$ modes were seen by Cahill and Leroi[13] at 2369 cm^{-1} and by Anderson et al.[14] at 2365 and 2374 cm^{-1}. It is not known what lattice modes of an argon matrix could couple with ν_s to give a Raman line. One could look much closer to the exciting line for evidence of lattice mode Raman scattering, but a double monochrometer is necessary

to remove enough of the intense unshifted Rayleigh scattered light such that one could unmask the weak lines close to the exciting line.

Another possibility is that the lines are spurious reflections and grating ghosts due to small imperfections in the spectrometer grating. Repeating the experiment at 5145.4 Å, another strong argon ion laser line would help distinguish between instrumental artifacts and real lines.

The very weak line at 2288.5 cm^{-1} corresponds quite nicely with that expected for ^{15}N-^{14}N which occurs in natural abundance ($\sim$0.7%) in $^{14}N_2$. The intensity ratio of this line compared to the line for $\nu_s(1\leftarrow0)$ is approximately 0.7% also. However, the S/N ratio of the line (<2) makes this assignment tentative. Hopefully, improvements in experimental technique will improve overall signal strength in future experiments.

The assignment of the line at 2279.8 cm^{-1} as $\nu_s(3\leftarrow2)$ was made with some reservation. The line appears >6 cm from the value calculated using gas phase vibrational constants while the other ν_s lines are within 3.5 cm^{-1} of their calculated values. However, with the assignments made in Table II, the vibrational line spacings in the matrix differ by approximately the same amount ($\sim$24 cm^{-1}). Thus, vibrational constants can be found[15] to describe the vibrational level spacings consistent with the form of the term symbol notation mentioned earlier.

Population of the upper vibrational levels in the X state of N_2 as evidenced by Raman lines originating from v=1 and v=2 suggests a very long vibrational relaxation time. Our next experiment was an attempt to obtain an order of magnitude estimate of this rate. The experiment involved watching the $\nu_s(2\leftarrow1)$ Raman signal build-up with time, possibly to

some steady-state value. The laser would then be turned off, allowing the excited molecules to relax, and then turned on again just long enough to obtain the new population of the v=1 state. We found that after approximately 100 minutes of excitation (5.2 watts at 4879.9 Å) the counting rate (~5800 counts/5 min) showed no apparent increase. We then turned the laser off and probed the population periodically for a five minute counting period. Figure 4 is a plot of log (counts/5 min) versus time (min). There is appreciable scatter in the data and the plot does not represent a very large change in the population of v=1. A least squares fit gives a slope of $7.1 \pm 1.2 \times 10^{-4}$ min^{-1}. Neglecting additional excitation during the probe period and repopulation of v=1 due to relaxation of molecules in v=2, this slope is the vibrational relaxation rate for molecules in v=1 returning to the ground state.

The lifetime $\tau(1/e)$ corresponding to this rate is 23 ± 3 hours! Obviously, this is a crude approximation due both to the assumptions made and the short data gathering period. Crucial points in this experiment are whether the counting rate really does level off and whether the "probing pulse" is exciting enough molecules to make the VR time appear longer than it really is. If steady-state can indeed be reached in 100 minutes, a VR time of 23 hours makes little sense at all.

To get a better estimate of the VR time, one should consider a more complete kinetic expression considering the time evolution of the population of both the v=1 and v=2 vibrational levels.

Figure 4. Log Raman (v=1) intensity versus t(min)

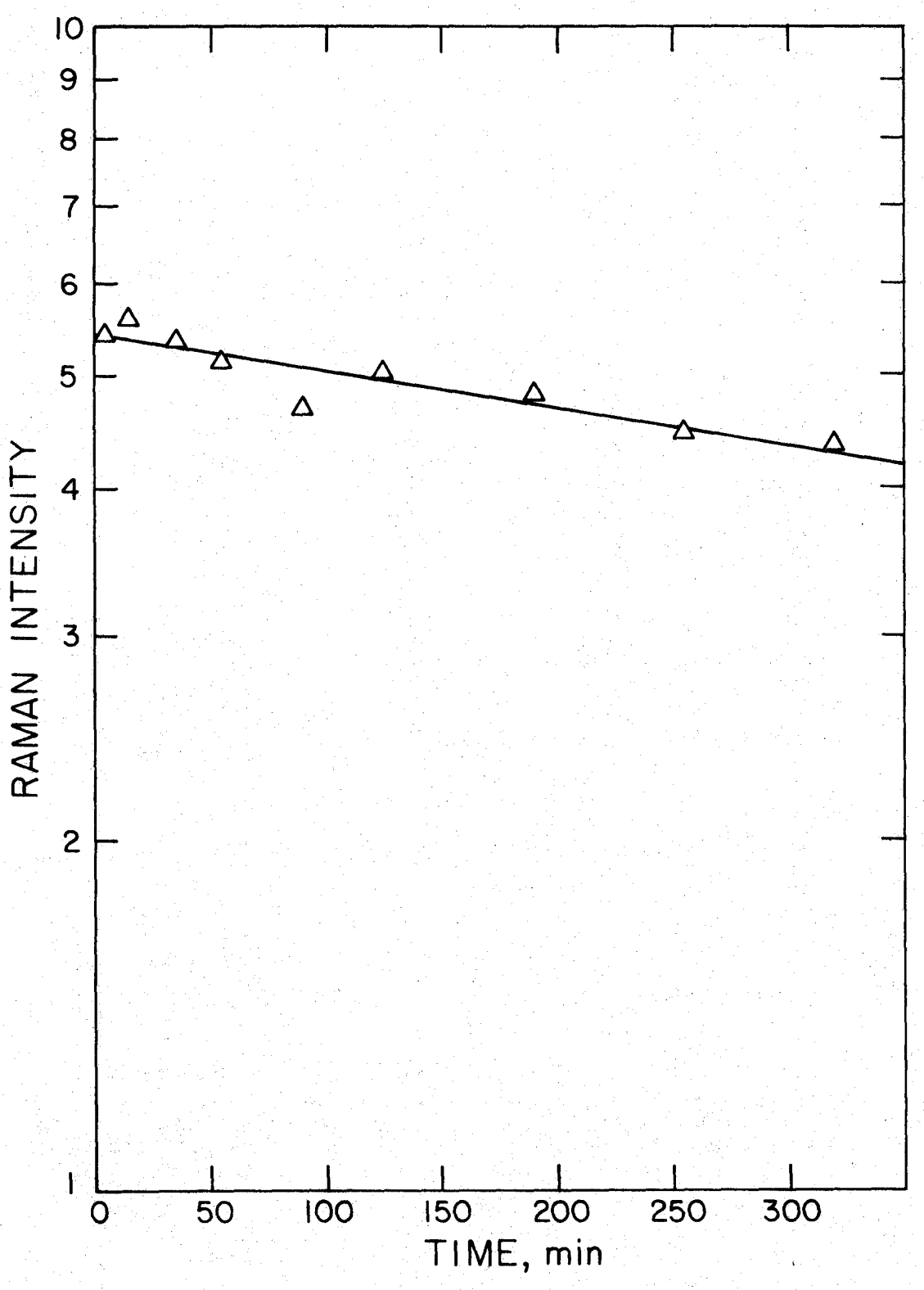

Proposed energy relaxation mechanism

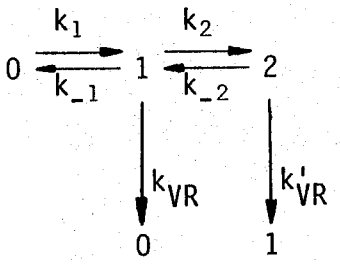

k_1 = rate constant for population of v=1 via Stoke's scattering.

k_{-1} = rate constant for return to v=0 via anti-Stoke's scattering.

k_2, k_{-2} = corresponding rate constants for v=2.

k_{VR}, k'_{VR} = vibrational relaxation rate constants.

Assumptions

a) Raman transition probability > with quantum number:[10] $k_2 \approx 2k_1$

b) $k_i \approx k_{-i}$

c) $k'_{VR} \approx k_{VR}$

The rate equation describing the time evolution of the population of v=1 is then

$$\frac{dP_1}{dt} = k_1 I_L P_0 + k_{-2} I_L P_2 - k_{-1} I_L P_1 - k_2 I_L P_1 - k_{VR} P_1 + k_{VR} P_2 \qquad (1)$$

where I_L = laser intensity (photons/cm^2 sec) and P_0, P_1, P_2 = populations of v=0, v=1, v=2 respectively. If P_1 can indeed achieve steady state value,

$$0 = k_1 I_L P_0 + 2k_1 I_L P_2 - k_1 I_L P_1 - 2k_1 I_L P_1 - k_{VR} P_1 + k_{VR} P_2$$

$$k_1 I_L (P_0 + 2P_2) = k_1 I_L (3P_1) + k_{VR} (P_1 - P_2) \qquad (2)$$

$$\frac{P_0 + 2P_2}{P_1 - P_2} = 3\,\frac{P_1}{P_1 - P_2} + \frac{k_{VR}}{k_1} \cdot \frac{1}{I_L} \qquad (3)$$

Now if experiments are done at different laser intensities and one monitors the intensity of the Raman lines after steady-state is reached and plots Equation (3), the slope should give

$$\frac{k_{VR}}{k_1}$$

where k_1 is simply the differential cross-section for Raman scattering. Hyatt et al.[16] measured this cross-section for N_2 in the gas phase and found it to be 6.8×10^{-30} cm^2 at 4880 Å. This value should be a reasonable estimate for N_2 in this environment since it is believed that rare gas matrices do not perturb their guest molecules appreciably.

A one point fit to Equation (3) was attempted using data from Figure 3. A k_{VR} of $\approx 6.0 \times 10^{-5}$ sec^{-1} was obtained corresponding to a lifetime $\tau_{VR}(1/e)$ of ≈ 5 hours. As of yet, this result is tentative because we have no evidence that the observed decay rate obeys our integrated rate equation (Equation 3).

Another way of manipulating Equation (1) provides a rate equation applicable for all times. It would be more desirable to use this approach if steady state could not be reached in a reasonable length of time.

When the laser is on, Equation (1) describes the time evolution of the population of v=1. However, when the laser is off, it simplifies to

$$\frac{dP_1}{dt} = k'_{VR}P_2 - k_{VR}P_1 \qquad (4)$$

If one considers v=2 the uppermost populated vibrational level, its population should follow the expression (laser off)

$$P_2(t) = P_2(0)e^{-k'_{VR}t} \tag{5}$$

Then Equation (4) becomes

$$\frac{dP_1}{dt} + k_{VR}P_1 = k'_{VR}P_2(0)e^{-k'_{VR}t} \tag{6}$$

This linear nonhomogeneous differential equation is easily solved.

$$P_1(t) = P_1(0)e^{-k_{VR}t} + \frac{k'_{VR}P_2(0)}{k_{VR} - k'_{VR}}\left(e^{-k'_{VR}t} - e^{-k_{VR}t}\right) \tag{7}$$

The vibrational relaxation rate constants can be extracted from Equation (7) by performing a nonlinear least squares regression analysis on a plot of $P_1(t)$ versus time. $P_1(t)$ is obtained by probing the Raman $\nu_{as}(0\leftarrow1)$ signal intensity periodically after initial excitation has provided a strong signal. This analysis was not performed on the data shown in Figure 4 because the change in signal strength over the period of data collection was too small.

The next set of experiments was aimed at obtaining a more accurate VR rate. The experiment whose results are shown in Figure 4 was repeated and an increase in signal strength with time was seen, contrary to the previous observation. This evidence suggests that the line could originate from the laser. A series of blank experiments, both with and without argon but no N_2, were run to see if the line did indeed originate from

the laser. Figure 5 is a scan over the Stoke's region for an argon matrix with an excitation power of 5 watts at 4879.9 Å. Figure 6 is a scan over the same region with no matrix and 460 mW of argon ion laser power at 4879.9 Å. Except for changes in intensity, the same lines appear in both experiments. When these figures are compared with Figure 3, close inspection reveals that laser plasma lines are responsible for all the unidentified lines as well as lines previously identified as $\nu_s(2\leftarrow1)$ and $\nu_s(3\leftarrow2)$ Raman transitions. The laser plasma lines disappear at low laser power (<50 mW) which is the reason why they were not observed in previous blank experiments.

Plagued by interfering laser plasma lines in the Stoke's region, experiments were then attempted in the anti-Stoke's region ($\nu_{as} = \nu_L + \nu_S$). Here the photomultiplier is approximately three times more sensitive and the spectrum should conclusively identify upper vibrational levels. Unfortunately, we found rather strong interference in this region from lines emitted by the laser also. Presumably, the laser cavity (>2 meters long) is acting as a waveguide for argon fluorescence or impurities in the discharge tube. To eliminate this problem, we placed a narrow-band (30 Å) interference filter in the path of the beam before it entered the dewar. The filter blocks to 10^5 on either side of the bandpass. However, it transmits only 60% at the peak so maximum available power is reduced to ~3 watts. Repetitive scans were made over the spectral region 4386 Å → 4380 Å at 0.25 Å/min. with an MCA dwell time of 1 min/channel. Figure 7 shows a sum of six separate scans. No assignment of the Raman transition $\nu_{as}(0\leftarrow1)$ expected near 2326 cm^{-1} is possible.

Figure 5. Scan over the Raman Stoke's region at 0.25Å/min.-channel with 5 watts of argon ion laser power at 4879.9Å. The matrix consists of a 4 hour deposit of argon.

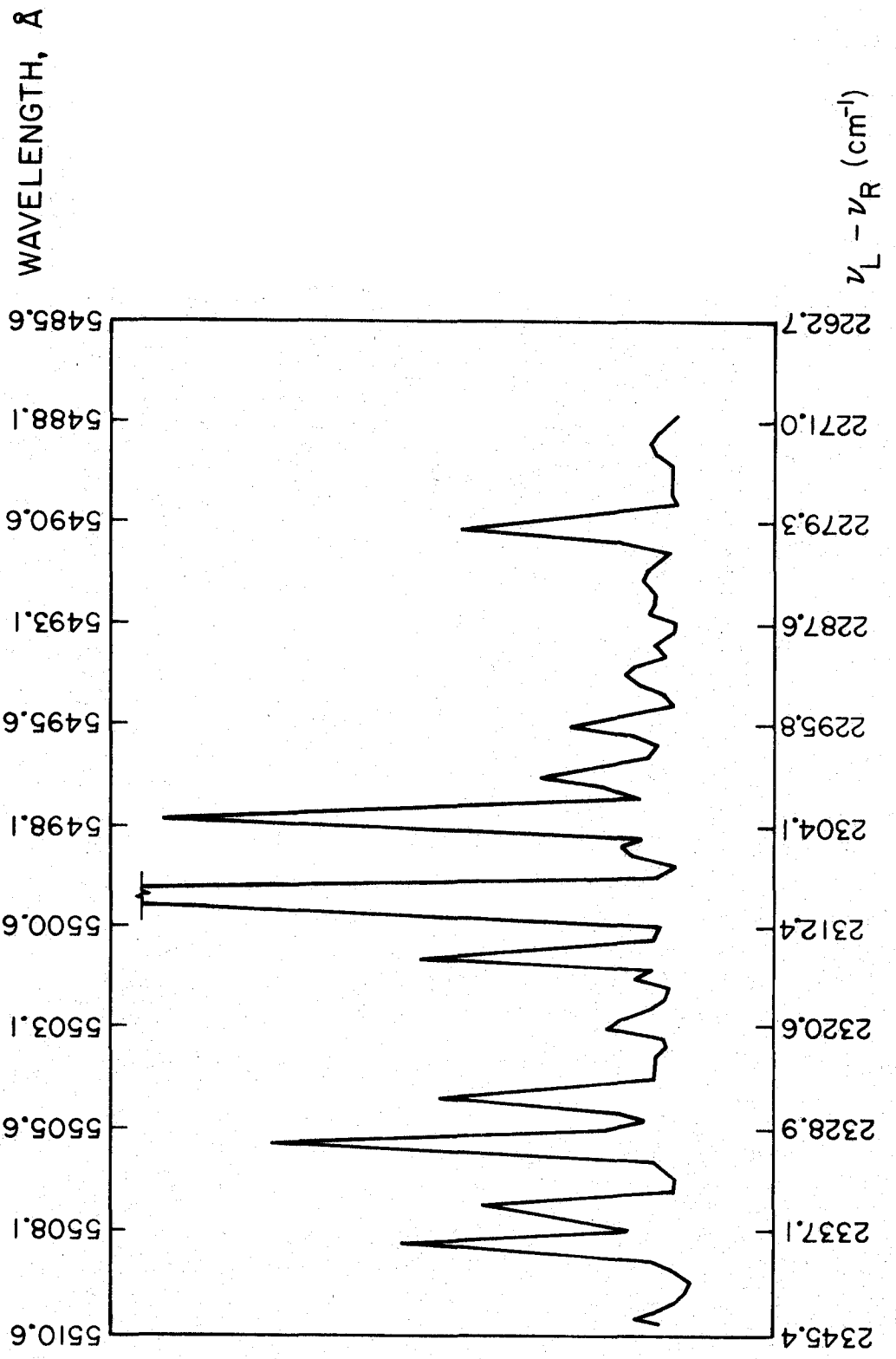
WAVELENGTH, Å
5485.6
5488.1
5490.6
5493.1
5495.6
5498.1
5500.6
5503.1
5505.6
5508.1
5510.6
$\nu_L - \nu_R$ (cm^{-1})
2262.7
2271.0
2279.3
2287.6
2295.8
2304.1
2312.4
2320.6
2328.9
2337.1
2345.4

Figure 5.

Figure 6. Scan over the Raman Stoke's region at 0.25Å/min.-channel with 460 mW of argon ion laser power at 4879.9Å. No matrix present.

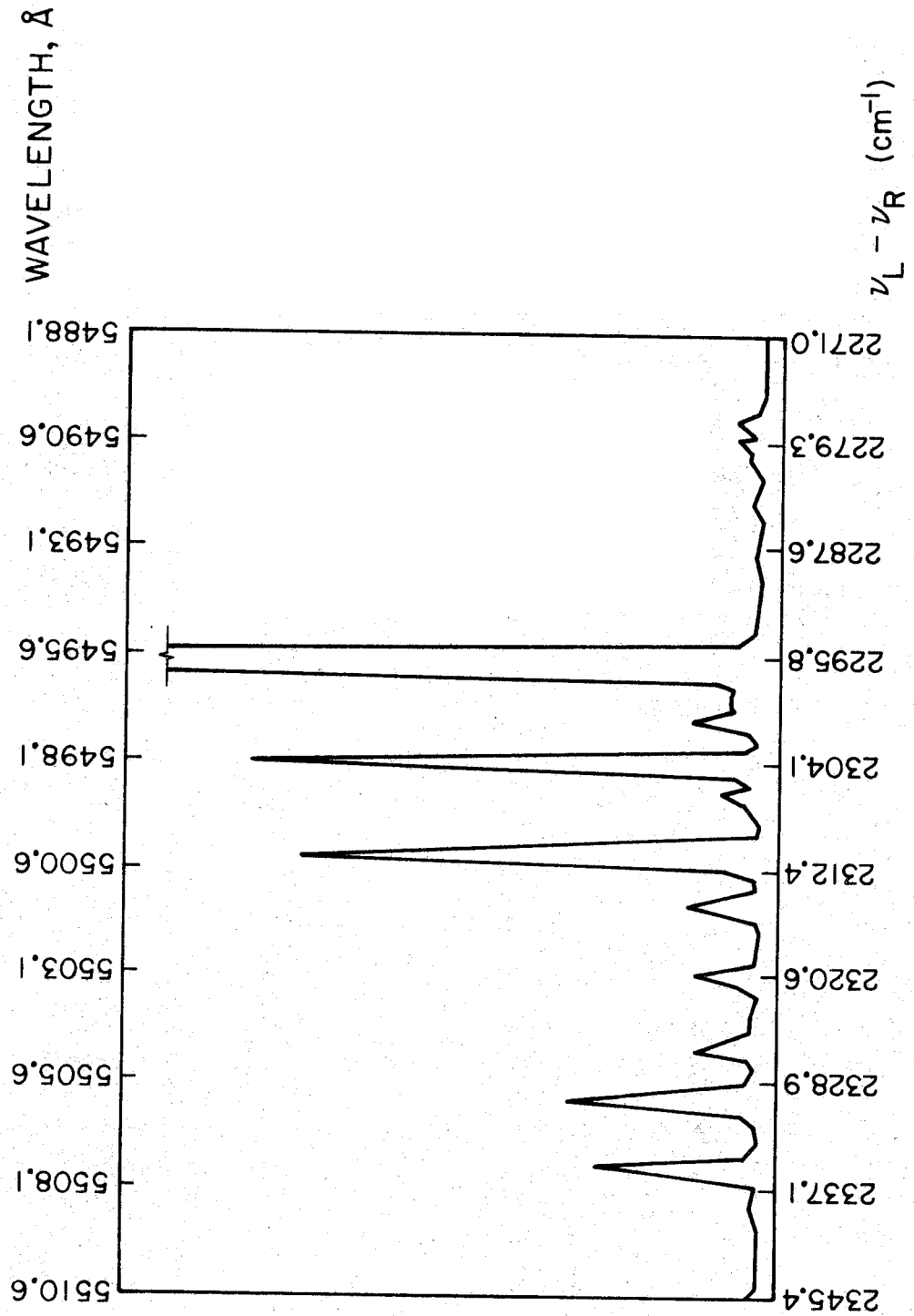
WAVELENGTH, Å
5488.1
5490.6
5493.1
5495.6
5498.1
5500.6
5503.1
5505.6
5508.1
5510.6
$\nu_L - \nu_R$ (cm^{-1})
2271.0
2279.3
2287.6
2295.8
2304.1
2312.4
2320.6
2328.9
2337.1
2345.4

Figure 6.

Figure 7. Multiple scans over the Raman anti-Stoke's region at 0.25Å/min.-channel with 3 watts of argon ion laser power (filtered) at 4879.9Å. The matrix consists of an 8 hour deposit of argon containing 1.0% N_2.

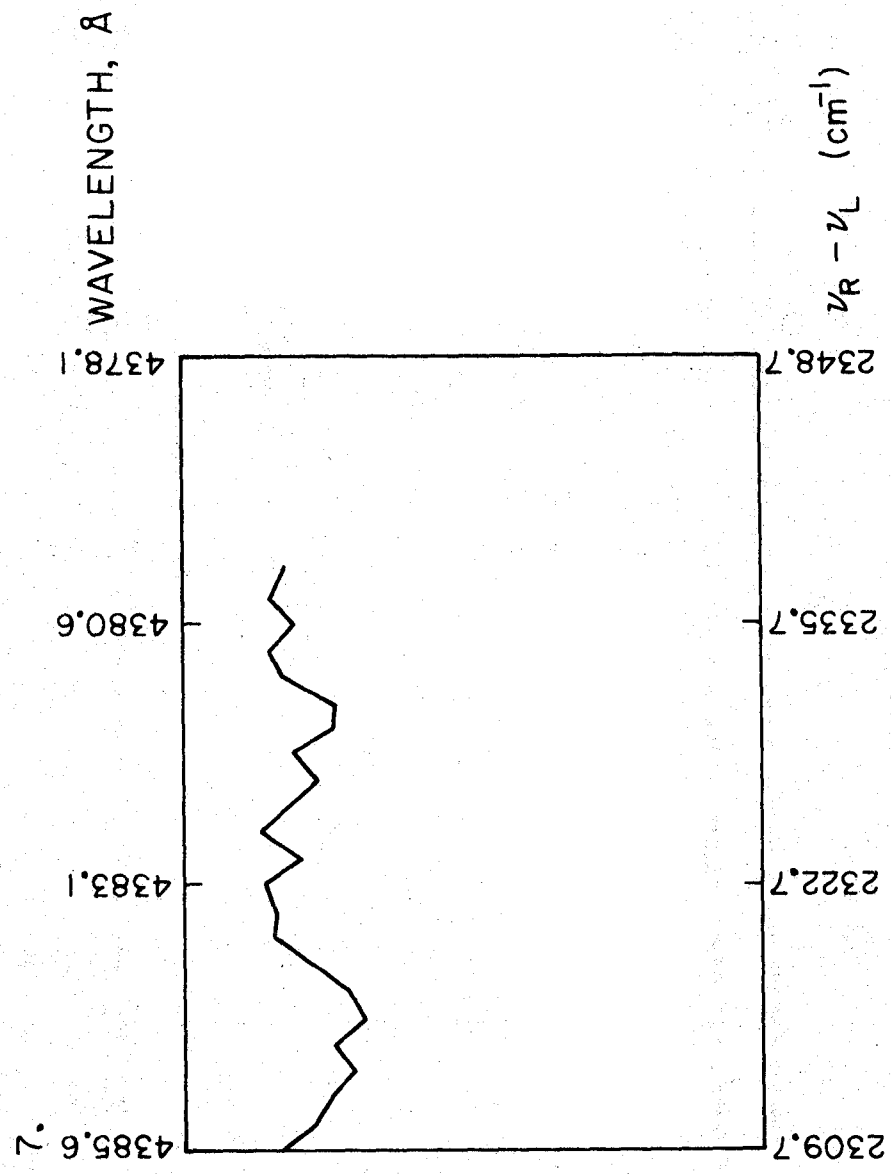
WAVELENGTH, Å
4378.1
4380.6
4383.1
4385.6
$\nu_R - \nu_L$ (cm^{-1})
2348.7
2335.7
2322.7
2309.7

Figure 7.

At this time, we decided to try experiments using 5145.4 Å argon ion laser excitation. Since there are no interfering laser plasma lines in the vicinity of expected $\nu_s(1\leftarrow0)$ and $\nu_s(2\leftarrow1)$ N_2 Raman Stoke's transitions, power robbing filters are not required and maximum excitation power (5W) is available.

Figure 8 is a low power blank scan over the Stoke's region with the positions of expected $\nu_s(1\leftarrow0)$ and $\nu_s(2\leftarrow1)$ N_2 Raman transitions indicated by arrows. Figure 9 is a scan for a seven-hour deposit of argon containing 0.85% N_2 over the same region. The intensity of laser plasma lines changes due to increased excitation power, however $\nu_s(1\leftarrow0)$ is clearly visible. Unfortunately, $\nu_s(2\leftarrow1)$ does not appear.

Figure 10 shows a low power blank scan over the anti-Stoke's region. Four of the strongest laser plasma lines were identified as specific argon ion transitions[17] and are marked as such. Here too, the position of the expected Raman transition $\nu_{as}(0\leftarrow1)$ is marked by an arrow. Figure 11 shows an anti-Stoke's scan for the same seven-hour deposit as in Figure 9. The laser plasma lines appear but still there is no evidence of $\nu_{as}(0\leftarrow1)$.

At this point, we did an experiment to test the effect of N_2 concentration. Hopefully, a matrix containing more N_2 would give a Raman $\nu_s(2\leftarrow1)$ Stoke's signal at a detectable level. Figure 12 shows a scan over the Stoke's region for an argon matrix containing 8.5% N_2. This four-hour deposit gave a $\nu_s(1\leftarrow0)$ Raman signal almost ten times that seen in Figure 9 where the matrix contained only 0.85% N_2. However, no evidence of a $\nu_s(2\leftarrow1)$ signal can be found. This is probably due to the greater probability of multiple site formation and lattice defects at higher concentration, both of which are thought to provide additional channels for VR.

Figure 8. Scan over the Raman Stoke's region at 0.25Å/min.-channel with 500 mW of argon ion laser power at 5145.4Å. No matrix present.

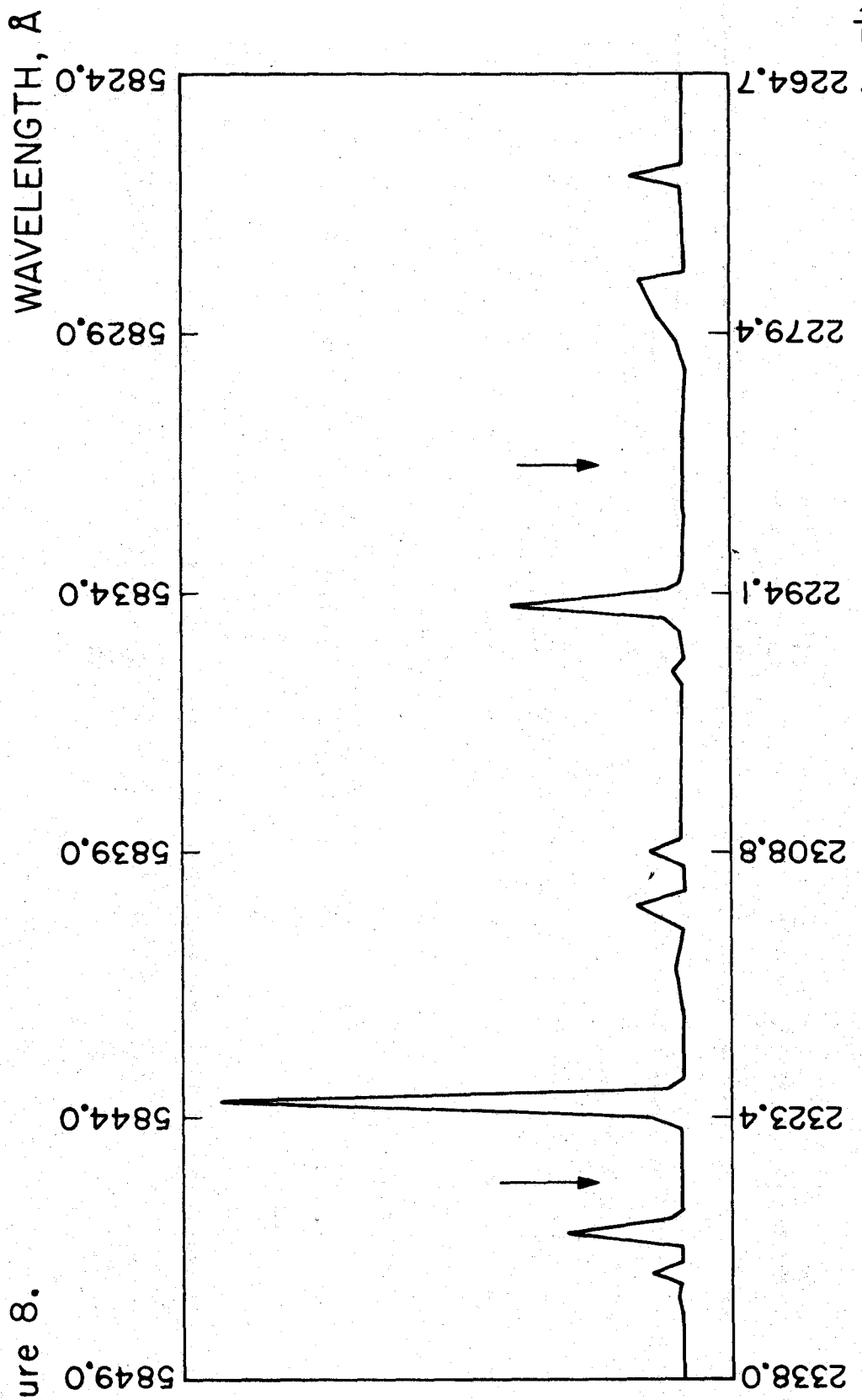
WAVELENGTH, Å
5824.0
5829.0
5834.0
5839.0
5844.0
5849.0
$\nu_L - \nu_R$ (cm^{-1})
2264.7
2279.4
2294.1
2308.8
2323.4
2338.0

Figure 8.

Figure 9. Scan over the Raman Stoke's region at 0.25Å/min.-channel with 5 watts of argon ion laser power at 5145.4Å. The matrix consists of a 7 hour deposit of argon containing 0.85% N_2.

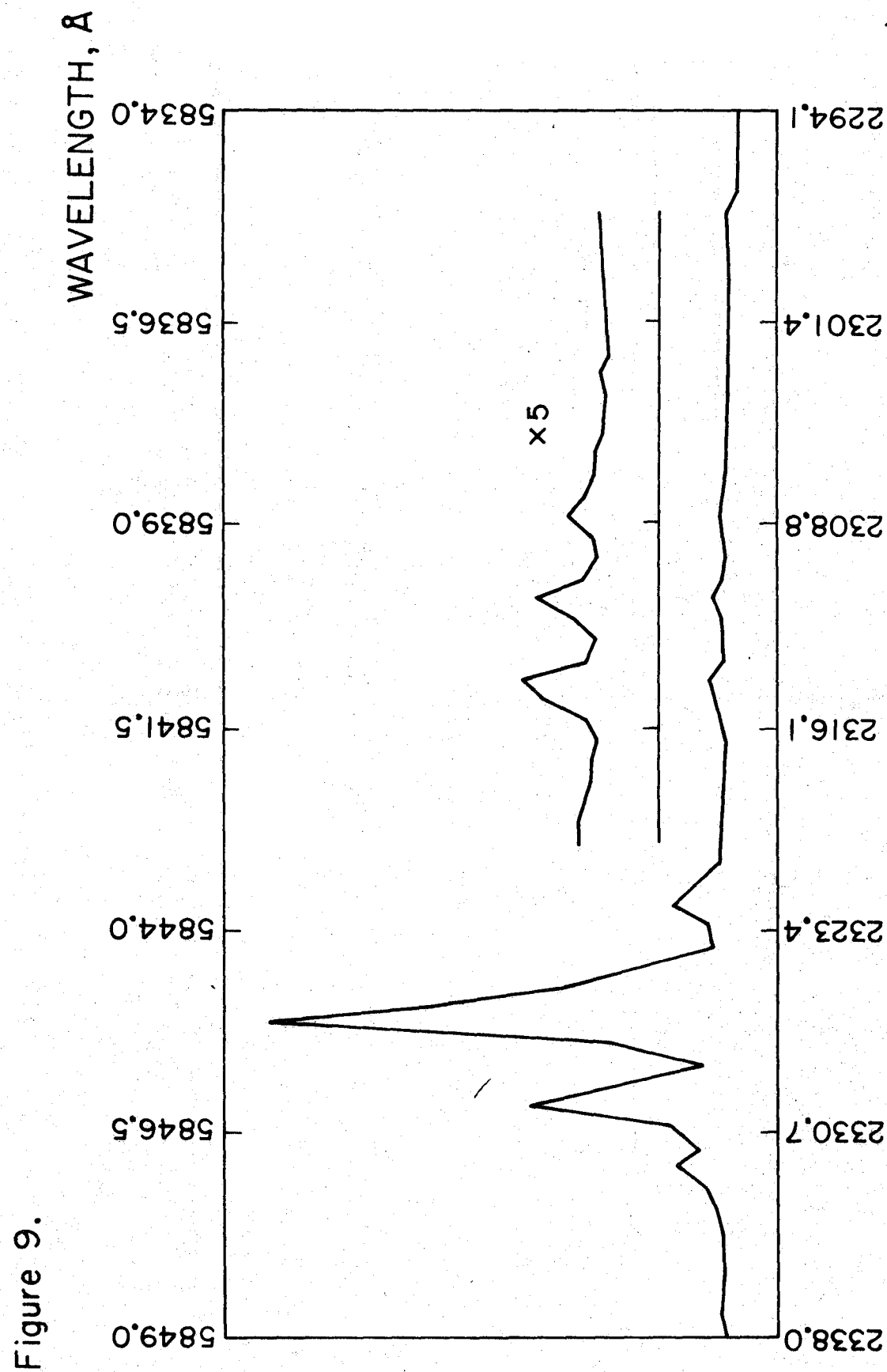
WAVELENGTH, Å
5834.0
5836.5
5839.0
5841.5
5844.0
5846.5
5849.0
$\nu_L - \nu_R$ (cm^{-1})
2294.1
2301.4
2308.8
2316.1
2323.4
2330.7
2338.0
×5

Figure 9.

Figure 10. Scan over the Raman anti-Stoke's region at 0.25Å/min.-channel with 500 mW of argon ion laser power at 5145.4Å. No matrix present.

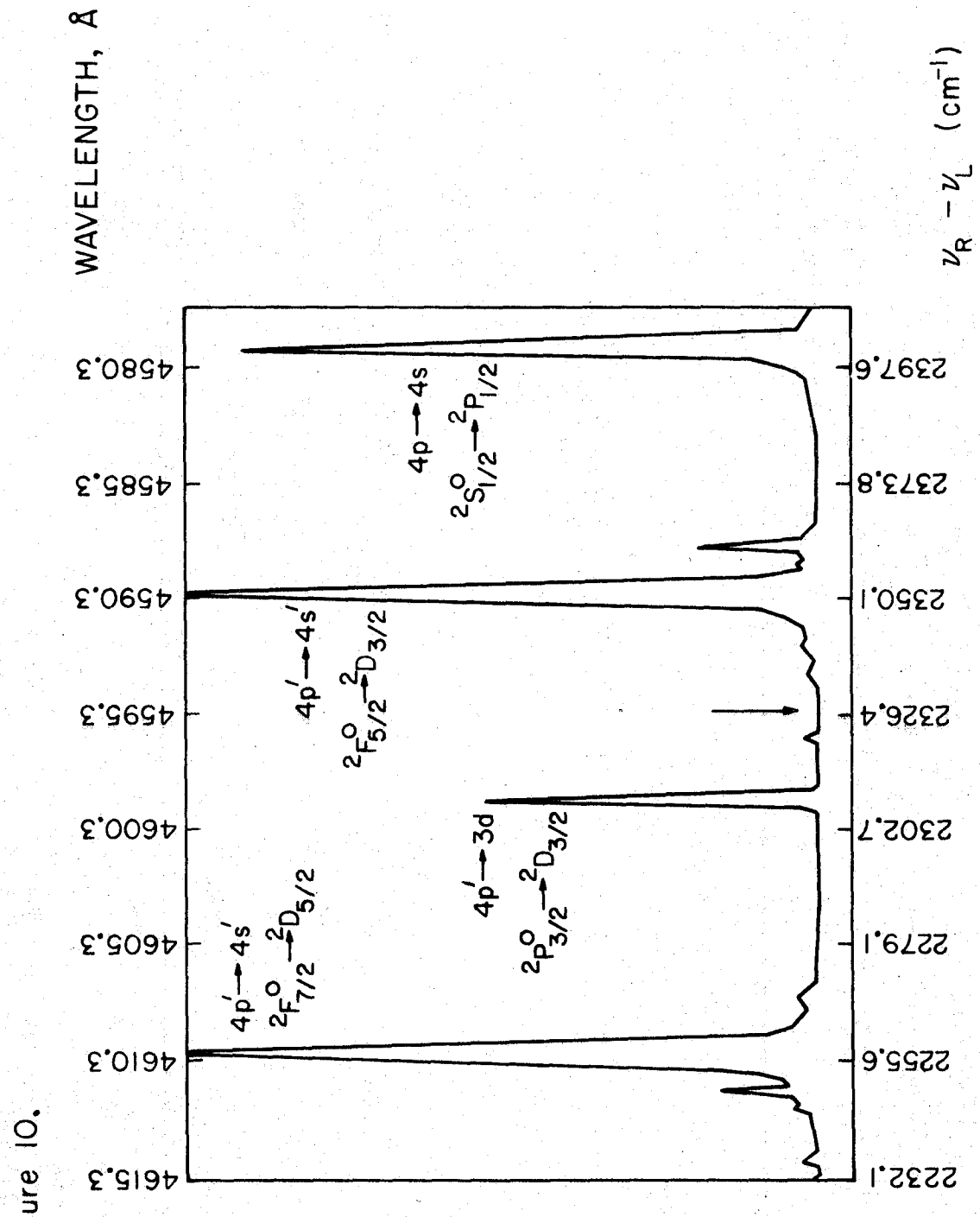
WAVELENGTH, Å
4615.3
4610.3
4605.3
4600.3
4595.3
4590.3
4585.3
4580.3
$\nu_R - \nu_L$ (cm^{-1})
2232.1
2255.6
2279.1
2302.7
2326.4
2350.1
2373.8
2397.6
4p′→4s′
$^2F^o_{7/2}$→$^2D_{5/2}$
4p′→4s′
$^2F^o_{5/2}$→$^2D_{3/2}$
4p→4s
$^2S^o_{1/2}$→$^2P_{1/2}$
4p′→3d
$^2P^o_{3/2}$→$^2D_{3/2}$

Figure 10.

Figure 11. Scan over the Raman anti-Stoke's region at 0.25Å/min.-channel with 5 watts of argon ion laser power at 5145.4Å. The matrix consists of a 7 hour deposit of argon containing 0.85% N_2.

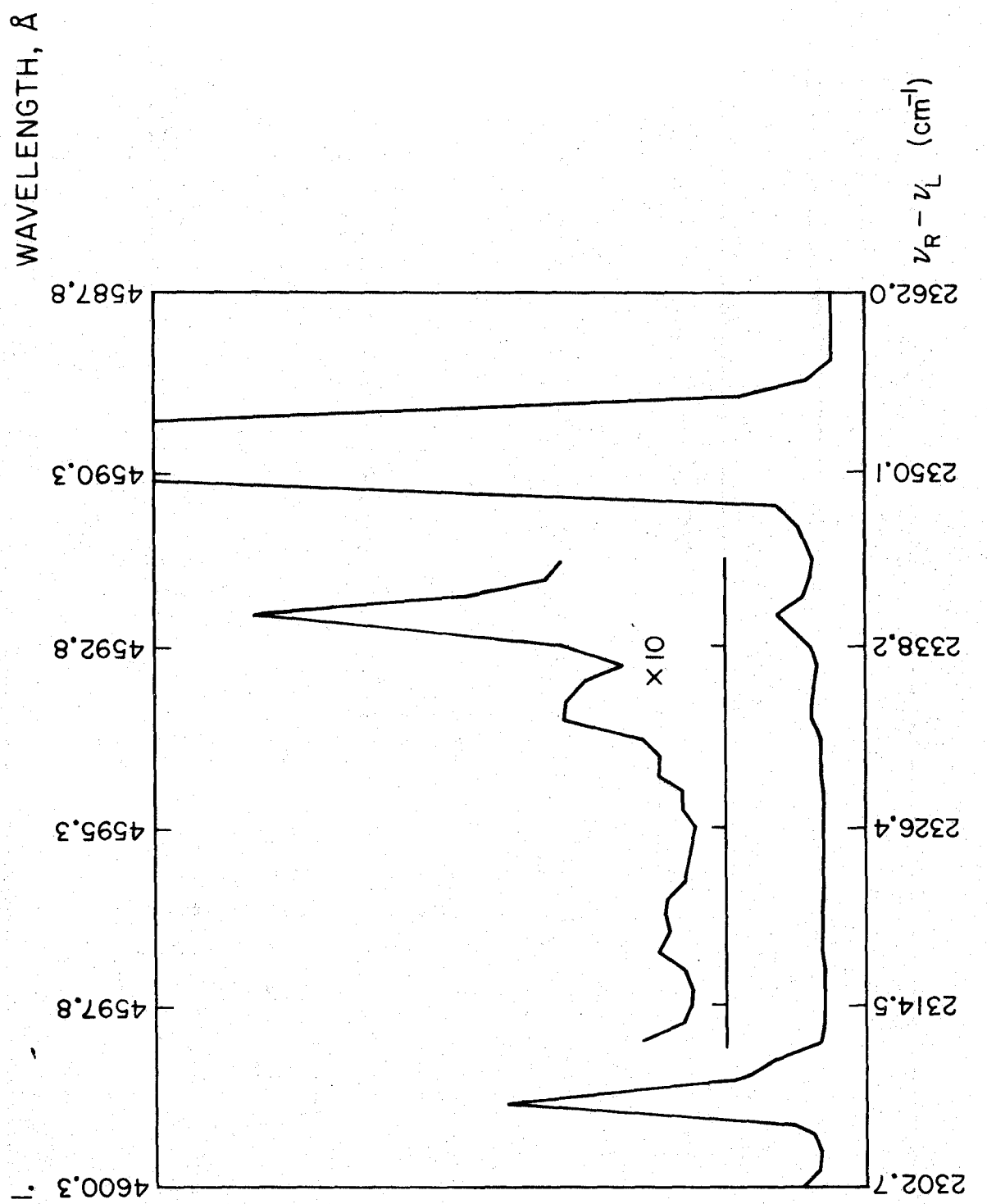
WAVELENGTH, Å
4587.8
4590.3
4592.8
4595.3
4597.8
4600.3
$\nu_R - \nu_L$ (cm^{-1})
2362.0
2350.1
2338.2
2326.4
2314.5
2302.7
×10

Figure 11.

Figure 12. Scan over the Raman Stoke's region at 0.25Å/min.-channel with 5 watts of argon ion laser power at 5145.4Å. The matrix consists of a 4 hour deposit of argon containing 8.5% N_2.

Figure 12.

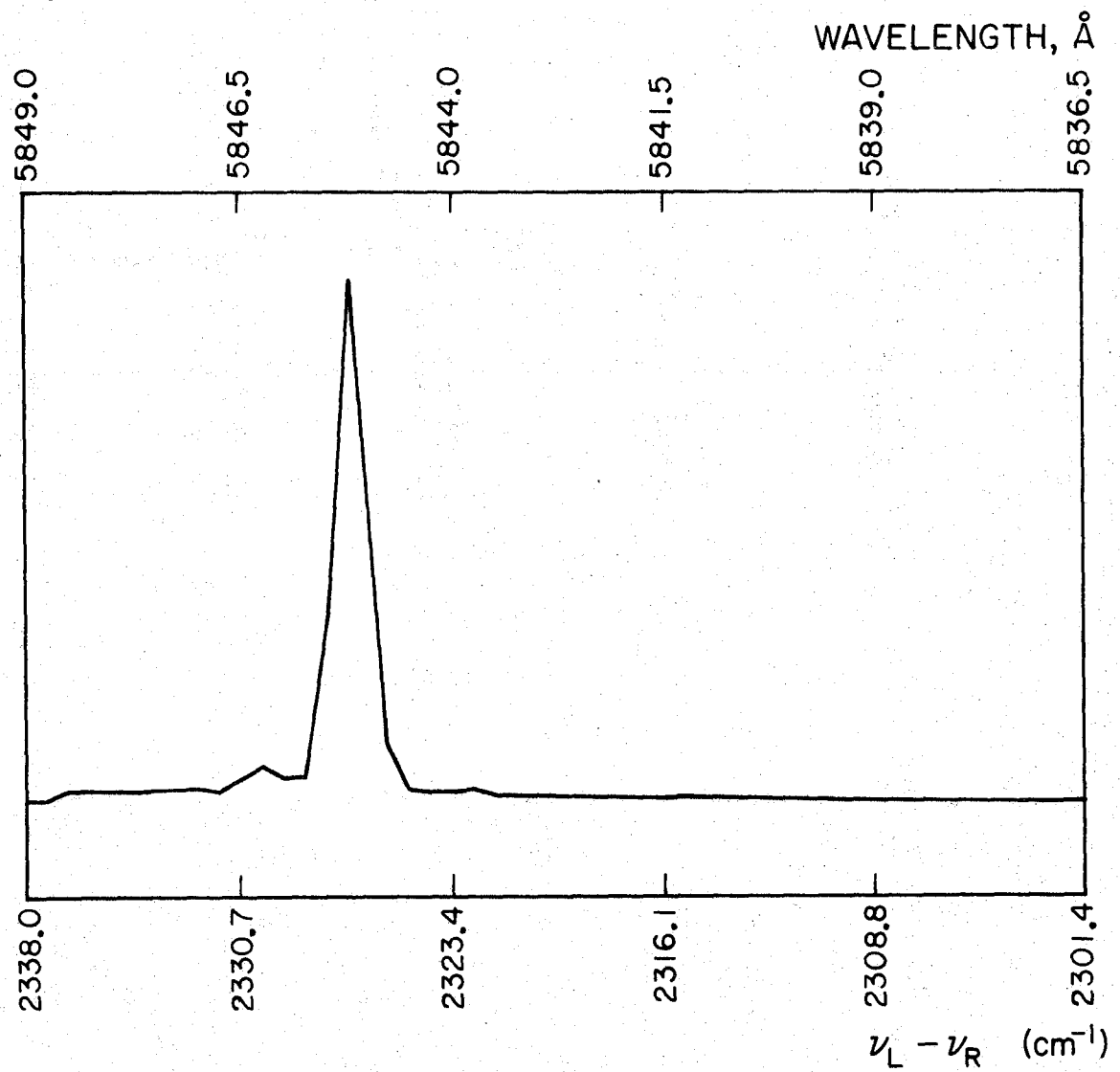
WAVELENGTH, Å
5849.0
5846.5
5844.0
5841.5
5839.0
5836.5
2338.0
2330.7
2323.4
2316.1
2308.8
2301.4
$\nu_L - \nu_R$ (cm^{-1})

Since all attempts at observing Raman scattering from upper vibrational levels of N_2 had failed using the maximum power available from the argon laser, we decided to try and stimulate the Raman process using the argon laser at 19,435.0 cm^{-1} (5145.4 Å) and a rhodamine 6G jet stream dye laser at 17,108.5 cm^{-1} (5845.2 Å), the Stoke's frequency. In this manner, we hoped to vibrationally excite N_2 molecules more efficiently. The process is illustrated schematically in Figure 13.

It was necessary to devise a new experimental configuration to attempt these stimulated Raman experiments. Figure 14 shows a schematic diagram of how the apparatus provides tunable two-frequency excitation. A diffraction grating (1200 grooves/mm) blazed at 5000 Å is used to remove unwanted plasma lines from the argon laser output. It has higher efficiency (67%, first order) than a narrow-band interference filter (∿55%). The right-angle prisms used for beam direction are anti-reflection (AR) coated. An achromatic lens (AR coated), which minimizes spherical and chromatic aberation, is used for optimum focusing of the two laser beams. It is aperatured, as well as the outside dewar window, to prevent unwanted reflections from entering the matrix chamber. The dye laser output is continuously monitored by an Epply thermo pile whose output is displayed on a Keithley microvolt meter and Leeds & Northrup strip chart recorder. Experiments are not begun until the dye laser output has remained stable for 30 minutes.

Before attempting to utilize a stimulated Raman process to improve excitation efficiency, calculations were performed to estimate possible gain. It was found that a gain of 10^4 over the spontaneous Raman intensity at the anti-Stoke's frequency should be realized (see Appendix I).

Figure 13. Energy level diagram for stimulated Raman process.

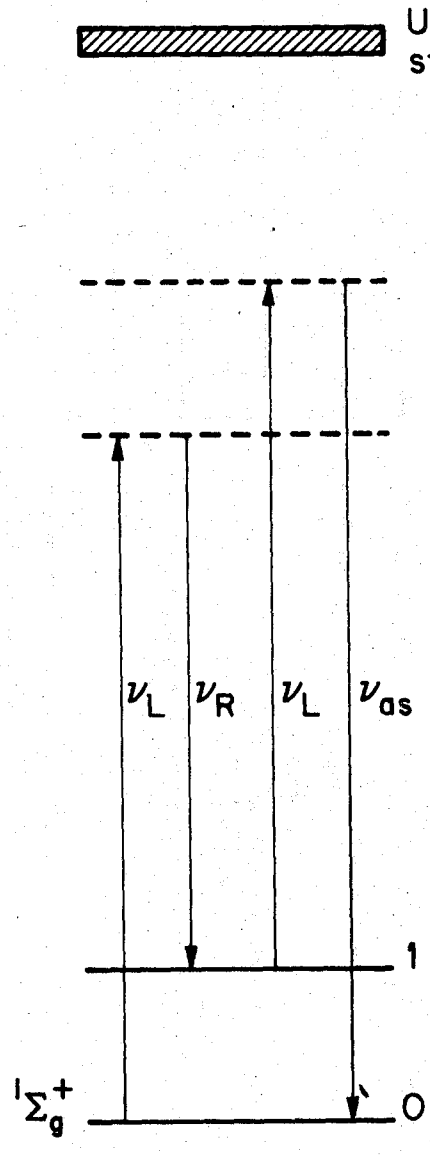

$$\nu_s = \nu_L - \nu_R$$

$$\nu_{as} = 2\nu_L - \nu_R$$

Figure 14. Schematic diagram of the apparatus for stimulated Raman experiment.

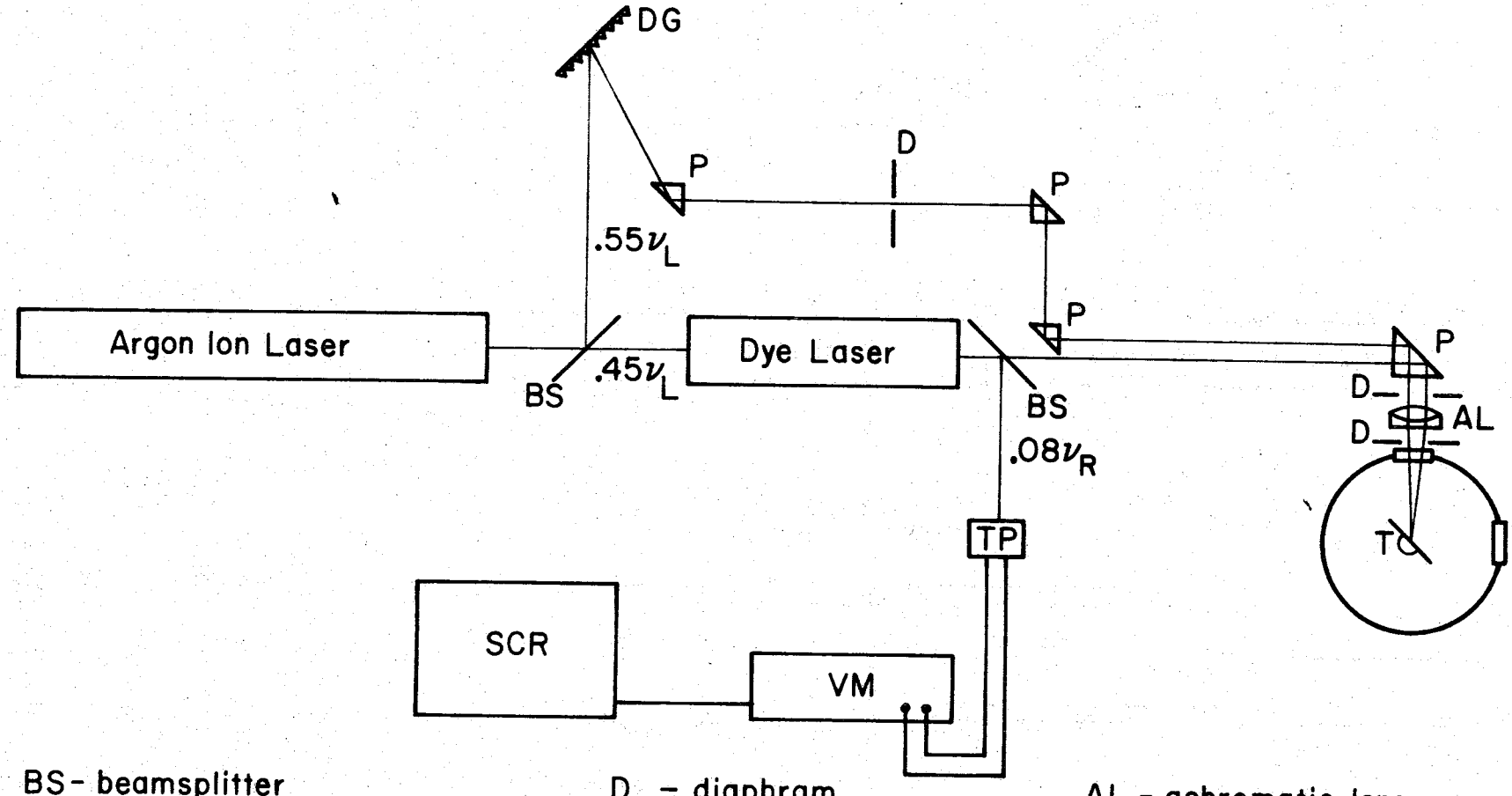

BS - beamsplitter
DG - diffraction grating
P - AR coated prism

D - diaphram
TP - thermopile
VM - voltmeter

AL - achromatic lens
T - target
SCR - strip chart recorder

All experiments involving both the argon and dye lasers are performed in the following manner. After the deposit has formed and the optics are aligned, a scan using only the argon laser is made over the Stoke's region to locate the $\nu_s(1\leftarrow 0)$ N Raman transition. This line consistently appears at 2326.5 ± 0.5 cm^{-1}. Then the argon laser is blocked and the dye laser is tuned to the Stoke's frequency (ν_R). This is accomplished by observing a maximum count rate with the spectrometer set at the position of $\nu_s(1\leftarrow 0)$. Upon completion of this tuning procedure, the matrix is then irradiated with both lasers while multiple scans over the anti-Stoke's region are made.

Figure 15 shows a scan over the Stoke's region for a 23-hour deposit of argon containing 0.85% N_2 using only 5145.4 Å argon laser excitation. The $\nu_s(1\leftarrow 0)$ N_2 Raman transition is quite strong. The dye laser was tuned to this frequency and Figure 16 shows the result of multiple scans over the anti-Stoke's region. No evidence of $\nu_{as}(0\leftarrow 1)$ appears. Figure 17 shows the result of a very slow scan (5 min/channel) over the anti-Stoke's region for a separate experiment involving a four-hour deposit (same matrix composition). Again, we had failed to provide sufficient excitation to observe $\nu_{as}(0\leftarrow 1)$.

Not being able to realize the expected gain in a stimulated process with our low power CW lasers, we decided to try and mode-lock the dye laser. Other groups[18,19] were able to realize 100 watt sub-picosecond pulses from CW pumped jet stream dye lasers similar to ours by adding 3,3' diethyl-oxadicarbocyanine iodide (DODCI) to rhodamine 6G.

After adding approximately 1 x 10^{-3} M DODCI to 5 x 10^{-3} M rhodamine 6G in ethylene glycol, we were able to mode-lock successfully at the

Figure 15. Scan over the Raman Stoke's region at 0.25Å/min.-channel with 1.3 watts of argon ion laser power at 5145.4Å. The matrix consists of a 23 hour deposit of argon containing 0.85% N_2.

Figure 15.

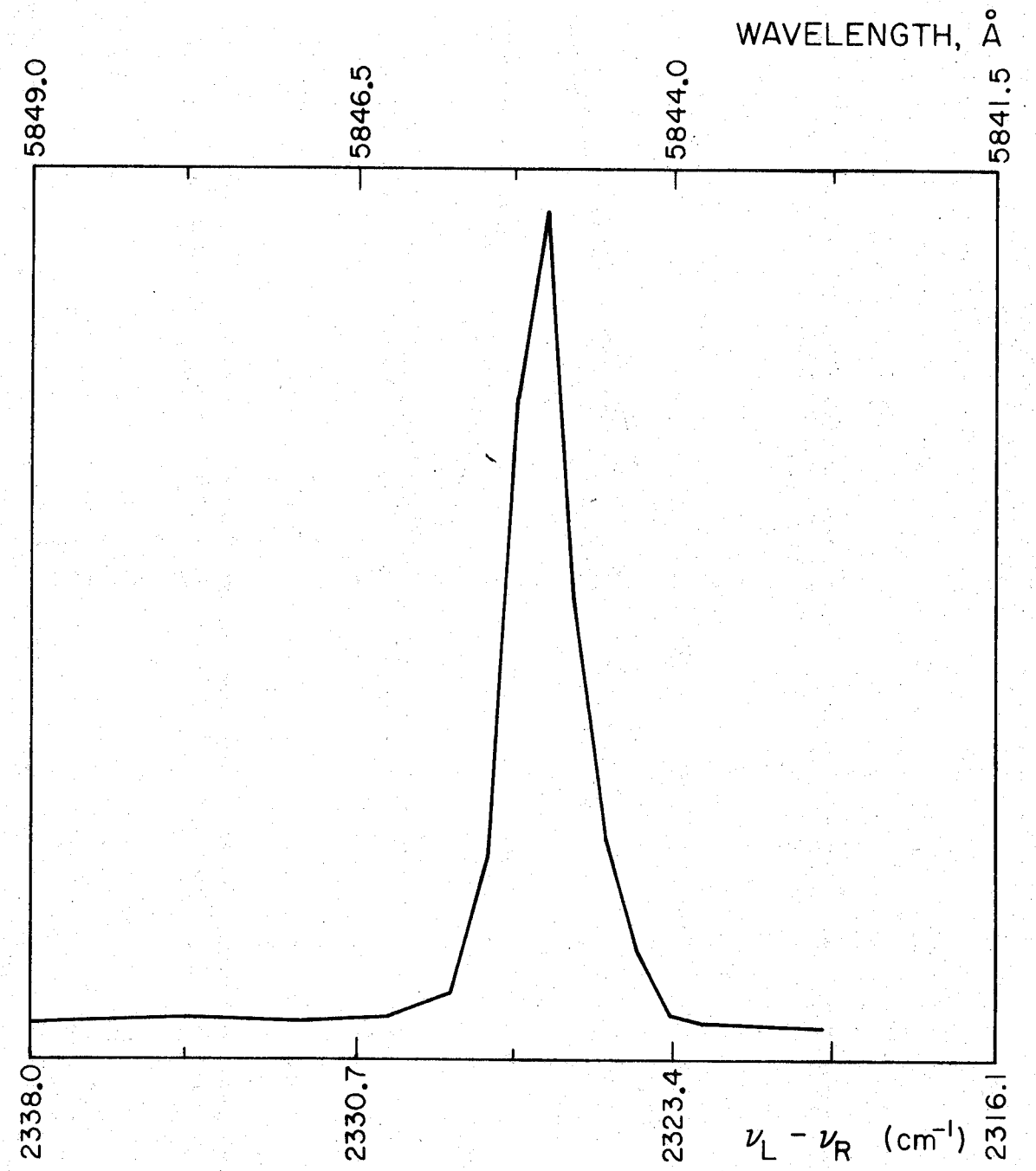
WAVELENGTH, Å
5849.0
5846.5
5844.0
5841.5
2338.0
2330.7
2323.4
2316.1
$\nu_L - \nu_R$ (cm^{-1})

Figure 16. Multiple scans over the Raman anti-Stoke's region at 0.25Å/min.-channel with 1.3 watts of argon ion laser power at 5145.4Å and 280 mW of rhodamine 6G dye laser power at 5845.0Å (Stoke's shifted 2326.3 cm^{-1}). The matrix consists of a 23 hour deposit of argon containing 0.85% N_2.

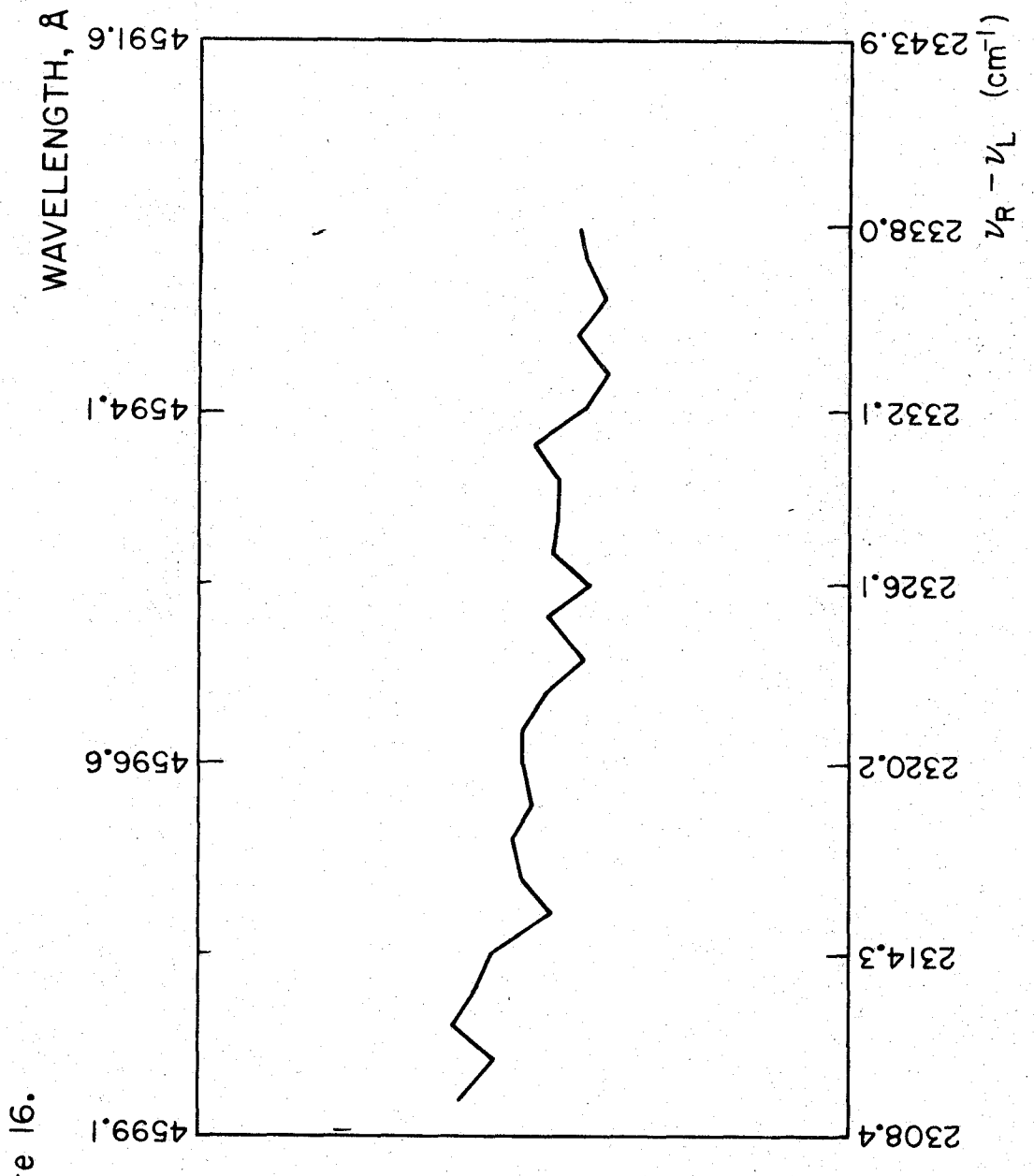
WAVELENGTH, Å
4591.6
4594.1
4596.6
4599.1
2343.9
2338.0
2332.1
2326.1
2320.2
2314.3
2308.4
$\nu_R - \nu_L$ (cm^{-1})

Figure 16.

Figure 17. Scan over the Raman anti-Stoke's region at 5 min./channel (channel width = 0.5Å) with 1.3 watts of argon ion laser power at 5145.4Å and 275 mW of rhodamine 6G dye laser power at 5845.2Å (Stoke's shifted 2326.9 cm^{-1}). The matrix consists of a 4 hour deposit of argon containing 0.85% N_2.

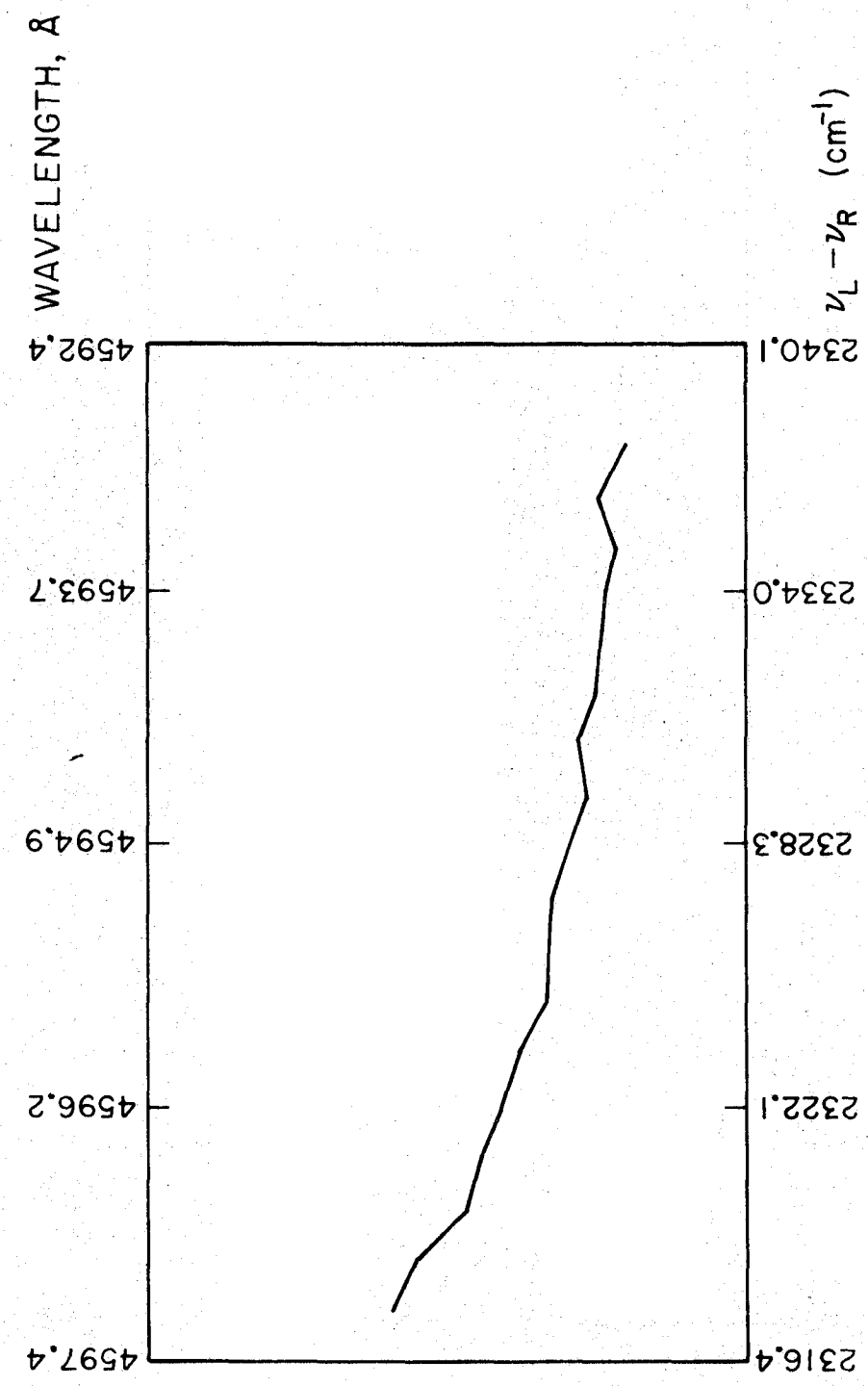
WAVELENGTH, Å
4592.4
4593.7
4594.9
4596.2
4597.4
$\nu_L - \nu_R$ (cm^{-1})
2340.1
2334.0
2328.3
2322.1
2316.4

Figure 17.

Stoke's frequency with 2.2 watts of 5145.4 Å argon pump power. Mode-locking would occur just above threshold only. With a fast silicon photodiode (terminated into 50 ohms) and a KS-1 Tektronix sampling unit, we were able to observe the pulse train as shown in Figure 18.

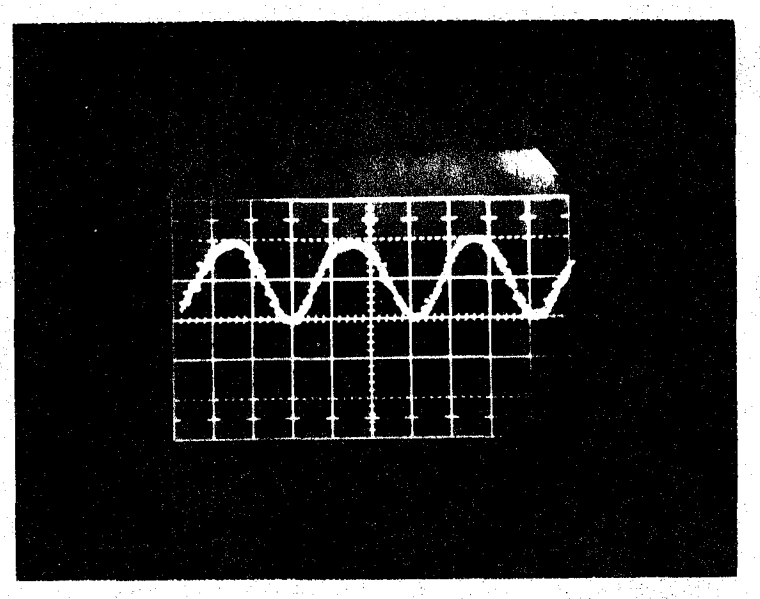

Figure 18. Mode-locked dye laser output at 5845.1 Å.

The oscilloscope trace was taken at 1 nsec/div horizontal and 50 mV/div vertical. The photodiode has a response time of a few nanoseconds so the pulse train has been convoluted into the photodiode response time. The pulses are separated by approximately 3.4 nsec (extrapolated baseline), which is just the cavity transit time of the dye laser. If we assume the pulse width is actually 1 psec, which others have seen[18,19], peak power is estimated to be 4.3 watts. Although much lower than we had hoped for,

we tried a few experiments anyway.

Figure 19 shows the result of multiple scans over the anti-Stoke's region for an eight-hour deposit of a matrix containing 0.85% N_2 with 1.3 watts of 5145.4 Å argon laser power and the dye laser mode-locked at 5845.1 Å (Stoke's shifted 2326.7 cm^{-1}). As in all previous attempts, no evidence of $\nu_{as}(0\leftarrow1)$ can be found. We simply do not have enough power to vibrationally excite N_2 such that Raman scattering from upper vibrational levels can be observed.

At this point, work on the project was stopped due to the failure of our equipment to provide sufficient excitation. Although we were not able to confirm a very long VR time for N_2 isolated in an argon matrix (as theoretical interpretations suggest), we have not ruled out a lifetime in the range of a few minutes (see Appendix II) which is certainly far longer than any ever seen before.

Figure 19. Multiple scans over the Raman anti-Stoke's region at 0.25Å/min.-channel with 1.3 watts of argon ion laser power at 5145.4Å and the dye laser mode-locked at 5845.1Å (Stoke's shifted 2326.7 cm^{-1}). The matrix consists of an 8 hour deposit of argon containing 0.85% N_2.

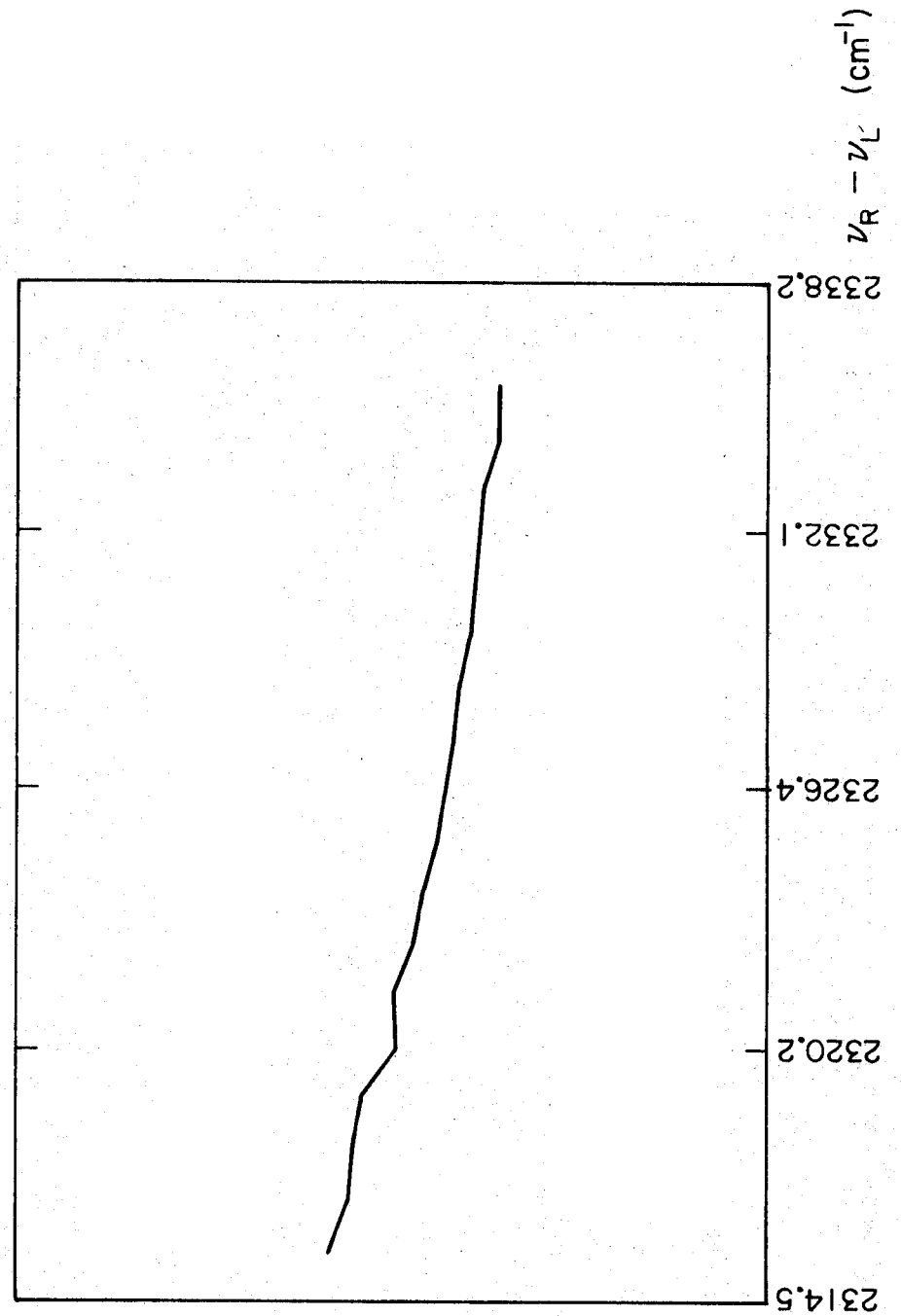

Figure 19.

VI. Discussion

The problem of vibrational relaxation in a solid environment has been investigated most recently by Nitzan and Jortner,[6,7] although some preliminary work in the area was done earlier by Sun and Rice.[4] After invoking a few simplifying assumptions, Nitzan and Jortner were able to formulate an expression for the relaxation rate of a diatomic molecule in a monatomic lattice from which the temperature dependence could be extracted. However, they were not able to identify the molecule-matrix coupling terms and so presently no a priori rate calculations are possible. A brief resume of their work is in order.

The discussion must begin with the simplifying assumptions they invoked. The first few are standard for matrix isolation experiments. Each guest molecule is isolated in a lattice site completely surrounded by matrix molecules and decays independently of the other guest molecules in the lattice. The molecule-matrix interaction is considered linear in intramolecular displacement. Rotations of the guest molecule are ignored and the medium is considered to be in thermal equilibrium during the relaxation process.

A Hamiltonian for the system was then constructed.[6]

$$H = \hbar\omega a^{\dagger}a + \sum_{\nu}\hbar\omega_{\nu}b_{\nu}^{\dagger}b_{\nu} + H_{mL} \qquad (4)$$

Here $a^{\dagger}$ and a are the creation and annihilation operators respectively for the guest diatomic treated as a harmonic oscillator with frequency ω.

The medium is considered a sum of harmonic oscillators with analogous operators $b_\nu^\dagger$, b_ν for each phonon frequency ω_ν.

The interaction term of the Hamiltonian takes the form[6]

$$H_{mL} = \sum_{\{\nu\}} \hbar\{G_{\{\nu\}} a^\dagger \Pi b_\nu + G^*\{\nu\} a \Pi b_\nu^\dagger\} \tag{5}$$

Here $G\{\nu\}$ are the coupling terms and $\{\nu\}$ refers to a collection of phonon states $\{1,2,\ldots,N\}$ such that energy is conserved ($\Sigma\omega_\nu=\omega$). This equation results from making the rotating wave approximation upon a system of linearly coupled oscillators. Terms of the form $a^\dagger b_\nu^\dagger$, ab_ν are neglected.

The equations of motion describing the system were set up in the Heisenberg representation

$$\dot{a} = \frac{i}{\hbar}[H, a]$$

$$\dot{b}_\nu = \frac{i}{\hbar}[H, b_\nu]$$

The equations were solved and from them resulted an expression for the relaxation rate of the guest molecule

$$\gamma(T) = \Pi\Sigma_\nu |G\{\nu\}|^2 p\{\nu\} \frac{e^{\beta\hbar\omega}-1}{\Pi_\nu (e^{\beta\hbar\omega_\nu}-1)} \tag{6}$$

Here $p(\nu)$ is the lattice density of state function and $(\beta=kT)^{-1}$. The temperature dependence comes out of an expression for the occupation number (thermally-averaged) of the individual lattice modes[6]

$$\langle n_\nu \rangle_T = \frac{1}{e^{\beta\hbar\omega_\nu}-1} = b_\nu^\dagger b_\nu \qquad (7)$$

Nitzan and Jortner's final expression involves replacing the sum over ν by a single collection of phonon states $\{\bar{\nu}\}$ which provides the smallest number of phonons consistent with $\sum_\nu \omega_\nu = \omega$ required for energy conservation.

There is very little data available to test the validity of the temperature dependence of Equation (6). Legay et al.[1] saw a factor of three decrease in the fluorescence lifetime of CO in an argon matrix upon increasing the temperature from 8 to 20° K. However, they were not confident enough in their temperature measurements to publish the data. Tinti and Robinson[3] saw very little change in the emission spectrum of $N_2A(^3\Sigma_u^+)$ upon temperature in the region 4-30° K which indicates a weak temperature effect upon the VR rate. Equation (6) predicts a factor of five increase in the VR rate for $N_2A(^3\Sigma_u^+)$ over the temperature region 4-30° K, contrary to experiment. This laboratory intended to do extensive temperature studies upon the VR rate of $N_2X(^1\Sigma_g^+)$ once the rate at 4.2° K had been accurately measured.

A priori rate calculations for these systems cannot be done until the molecule-matrix coupling terms $G(\nu)$ are understood.

An energy gap law[7] has been proposed by Nitzan and Jortner as a starting point in the understanding of these terms. They propose that the coupling terms take the form $G(\nu) = Cb^{\omega/\omega_\nu}$ so that the VR rate becomes

$$\gamma = Ab^{2\omega/\omega_\nu}$$

Here A and b are constants for a given temperature with the constraint that ($0<b<1$) and ω_ν is taken near the maximum in the phonon density of states function.[20] A plot can be made of log γ versus ω having slope

$$\frac{2}{\omega_\nu} \log b$$

and intercept log A. A crude upper bound for A can be obtained by examining this equation as $\omega \to 0$. As the diatomic vibrational frequency ω approaches the lattice mode frequencies ω_ν, the VR rate should achieve its maximum value.

At 4.2°K, typical spectral line widths in a matrix are $\tilde{\sim}3$ cm^{-1}.[3,21] If lifetime broadening were responsible for the entire width and the VR time governed the lifetime of the vibrational level, then the VR rate would be $\tilde{\sim}10^{+11}$ sec. Certainly this is an upper limit for A. A plot of log γ = 2log b/ω_ν + log A is shown in Figure 20, drawn such that the line passes through the known VR rate of $N_2A(^3\Sigma_u^+)$ and the crude estimate of log A found above. Using 60 cm^{-1} for ω_ν, which is near the Debye cutoff for argon, b has a value of 0.6. An arrow has been placed at the stretching frequency for $N_2X(^1\Sigma_g^+)$. One immediately sees that a VR time of over 400 hours is predicted by this plot for N_2 in its ground electronic state! Although this is an unreasonable result, it does not indicate that the form of the coupling terms is completely wrong since in estimating an A value it was assumed that lifetime broadening was responsible for the entire spectral line width. Certainly, molecule-matrix coupling contributes

Figure 20. Log VR rate versus vibrational stretching frequency

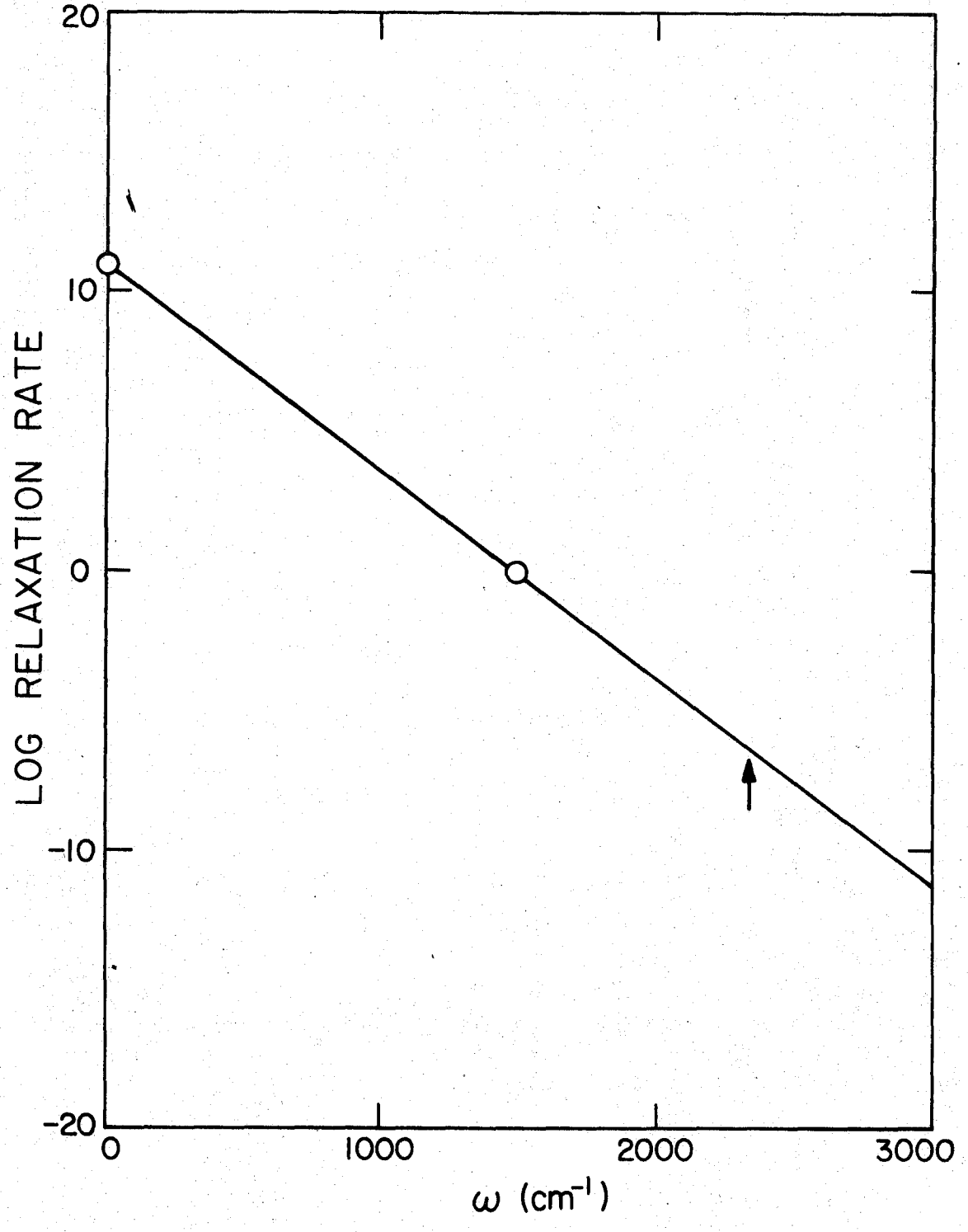

something to the observed line width and inhomogeneous broadening is common in matrix isolation experiments due to differences in individual substitutional sites. Until many more experiments have been done, a more quantitative form of the coupling terms involved can not be obtained.

An upper limit to the observed vibrational relaxation time of a diatomic must be determined by all other decay processes available. One must consider the radiative lifetime for both dipole and quadrupole emission. In all homonuclear diatomic molecules, the dipole moment is zero and thus dipole emission is strictly forbidden. However, N_2 does have a quadrupole moment[22] (-1.52×10^{-26} e.s.u. cm^2) and, if the selection rules are satisfied (see Table III), electric quadrupole emission is allowed.

Table III. Selection Rules for Quadrupole Emission[11]

symmetry	$g \longleftrightarrow g$
	$u \longleftrightarrow u$
	$g \nleftrightarrow u$
	$+ \longleftrightarrow +$
	$- \longleftrightarrow -$
	$+ \nleftrightarrow -$
rotation	$\Delta J = 0, \pm 2$
	$J = 0 \nleftrightarrow J = 0$

The Einstein transition probability for spontaneous quadrupole emission[23] from state n to state m is

$$A_{nm} = \frac{32\pi^6 \nu_{nm}^5}{5h(2J_n + 1)} |\langle n|Q_{zz}|m\rangle|^2$$

Here Q_{zz} is the instantaneous quadrupole moment having the form[24]

$$Q_{zz}(R) = \tfrac{1}{2} \int (3z^2 - r^2)\rho(r;R)dr$$

Recent calculations of the vibrational matrix elements of the quadrupole moment necessary to obtain the quadrupole transition probabilities were performed by Cartwright and Dunning[24] for N_2 using generalized valence bond wavefunctions.

Their matrix elements took the form[24]

$$\langle \nu'J'|Q_{zz}|\nu J\rangle = \int_0^\infty \phi^*_{\nu'J'}(R)Q_{zz}(R)\phi_{\nu J}(R)dR$$

Converting their values from atomic units to cgs units for the first two vibrational levels of N_2 in its ground state, the following transition probabilities for spontaneous quadruple emission were obtained

$$A_{10} \approx 2.0 \times 10^{-8} \text{ sec}^{-1}$$
$$A_{20} \approx 2.5 \times 10^{-9} \text{ sec}^{-1}$$
$$A_{21} \approx 3.7 \times 10^{-8} \text{ sec}^{-1}$$

The mean radiative lifetime for quadrupole emission from vibrational state n is then simply the reciprocal of the corresponding A_{nm} value. Thus,

$\tau_1 \approx 5 \times 10^7$ sec and $\tau_2 \approx 3 \times 10^7$ sec.

Herzberg states that quadrupole emission transition probabilities are typically 10^{-8} times those of strongly allowed dipole transitions.[11] To verify this generalization, one can compare the A_{10} value found for N_2 with the dipole emission transition probability for HCl.

Herbelin and Emanuel report a value of 34.6 sec^{-1} for the A_{10} value of HCl.[23] Thus, the ratio of quadrupole to dipole emission probabilities for N_2/HCl is $\approx 10^{-9}$.

Cartwright and Dunning's calculations on N_2 have provided estimates of $\approx 7 \times 10^3$ hours and $\approx 1 \times 10^4$ hours for the radiative lifetimes of v=2 and v=1 in N_2 respectively! It is expected that the perturbation of the matrix upon N_2 will cause the quadrupole radiative lifetime to be much less than the calculated estimates.

There is not much experimental evidence from which the perturbation of the matrix upon the lifetime of quadrupole emission can be determined. IR absorption of N_2 has been seen in the gas phase under high (60 atm) pressure by Crawford et al.[25] and in the liquid phase by Oxholm and Williams.[26] In both cases, absorption was considered to be due to "enforced dipole radiation" involving collision induced dipole moments. No evidence for IR absorption by N_2 was seen by Becker and Pimentel[27] when solid N_2 was used as a host for matrix-isolation experiments on the hydrogen halides.

The only conclusive way to determine if the matrix perturbation upon N_2 is strong enough to make quadrupole emission an important decay channel for excited ($v \geq 1$) nitrogen would be to check in the IR for the 1→0, 2→0, etc. emission lines. If seen, the radiative lifetimes corresponding to

the intensities of the emission lines would be upper limits to the observed vibrational lifetimes from the Raman experiment. If the matrix perturbation upon the radiative lifetime is small, our crude estimate of a few minutes for the VR time of N_2 (v=1) is not beyond reason since the radiative lifetime is much longer.

VII. Conclusion

The Raman spectra of $N_2(^1\Sigma_g^+)$ we obtained did not provide conclusive evidence of scattering from upper vibrational levels. If more excitation power was available at a wavelength closer to resonance with allowed electronic transitions (where the Raman process is more efficient), then the techniques we used should provide an accurate determination of the VR time for N_2 isolated in an argon matrix.

Once the VR rate is obtained at 4.2°K, of special interest will be the temperature dependence of the VR rate. Nitzan and Jortner's theory predicts a factor of five or more increase in the VR rate between 10 and 22°K.

The effect of the host matrix might also prove interesting. From Figures 21-23, one can see that although argon, krypton, and neon have similar phonon frequency distributions, the position of the maximum density of states differs

$$\text{argon} \approx 62\ \text{cm}^{-1}$$
$$\text{neon} \approx 50\ \text{cm}^{-1}$$
$$\text{krypton} \approx 45\ \text{cm}^{-1}$$

Thus, if the energy gap law is indeed correct and the coupling term sum can be approximated by one term containing a single collection of phonon states near the density of states maximum, then the VR rate will be substantially slower in krypton and neon than in argon.

An isotope effect is possible for N_2 as well. The stretching vibration for ^{15}N-^{14}N is approximately 40 cm^{-1} smaller than that of $^{14}N_2$. This

Figure 21. Phonon frequency distribution[28] for argon.

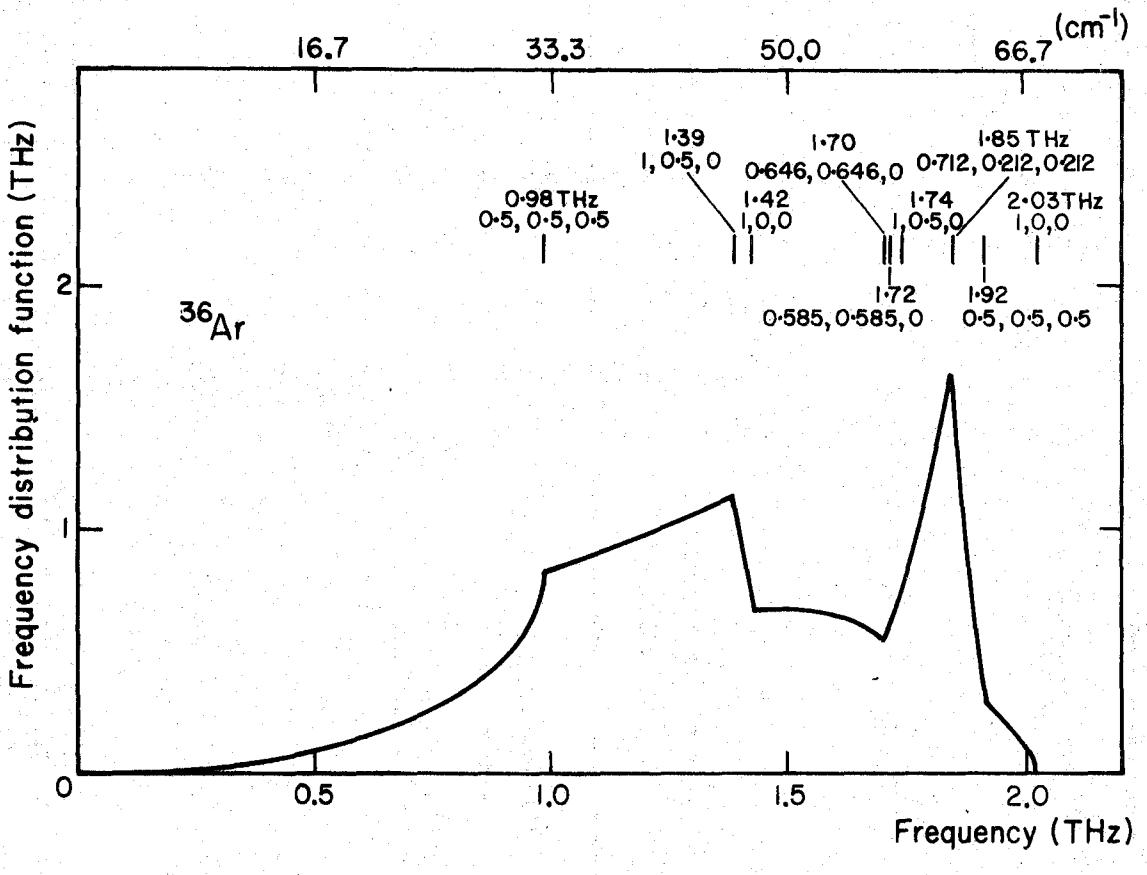

Figure 22. Phonon frequency distribution[29] for krypton.

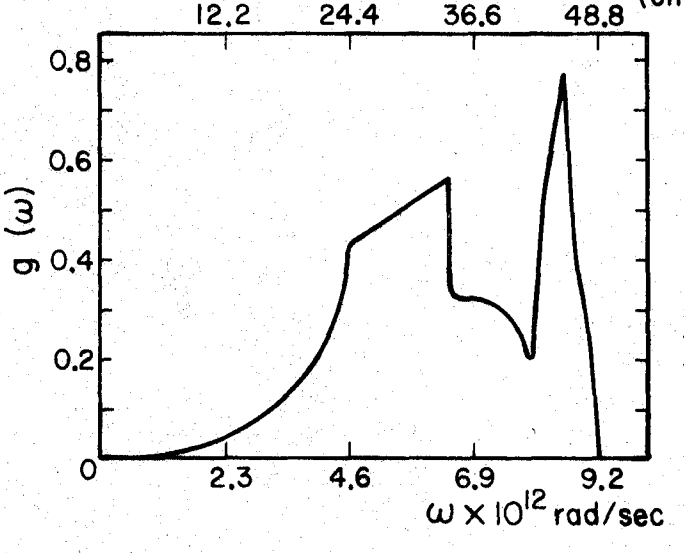

Figure 23. Phonon frequency distribution[30] for neon.

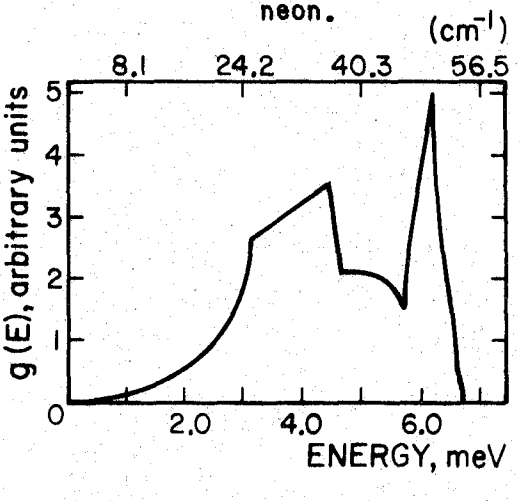

alone should mean a faster VR rate. On top of this is another perturbation, perhaps even more important. In ^{15}N-^{14}N, the center of mass is slightly displaced from the center of charge. The effect this would have on the radiative transition probability should be noticeable, further increasing the observed decay rate.

Finally, a concentration study would provide additional important data. The rate of excitation is concentration dependent. Increasing the concentration of N_2 should give larger Raman signals. However, as the concentration of N_2 increases, other channels for VR involving multiple sites and lattice defects might become important.

In conclusion, there is a wealth of information to learn about energy transfer in this system.

VIII. Appendix I

An estimate of possible gain a stimulated Raman process can provide over the normal spontaneous Raman process can be obtained by comparing expected signal strength for each phenomenon.

The stimulated Raman process we have attempted to utilize has been called "three-wave mixing"[33] by physicists and also "coherent anti-Stoke's Raman"[34] by others. Briefly, it is considered to be an interaction of the laser field at ν_L with the Stoke's field at $\nu_R(\nu_R = \nu_L - \nu_s)$ through the third order nonlinear susceptibility $\chi^{(3)}$ to generate polarization at $\nu_{as} = 2\nu_L - \nu_R$, the anti-Stoke's frequency.

The intensity of the stimulated anti-Stoke's signal has been shown to follow the expression[34]

$$I(\nu_{as})_{stim} = 2.77 \times 10^{-3} \frac{d^2 |N_0 \chi^{(3)}|^2 I(\nu_L)^2 I(\nu_R)}{n^4 \lambda_{as}^2 \sigma^2} \qquad (8)$$

Here d is the medium thickness (cm), N_0 is the molecular density (cm^{-3}), n is the index of refraction, λ_{as} is the anti-Stoke's wavelength, and σ is the laser beam cross section. All intensities are expressed as photons/sec and frequencies are in hertz. At resonance ($\nu_L - \nu_R = \nu_s$) the third order nonlinear susceptibility $\chi^{(3)}$ takes the form[34]

$$\chi^{(3)} = \frac{2\pi^2 c^3}{\nu_R^3 \Gamma_R} (d\alpha/d\Omega) \qquad (9)$$

In this expression $(d\alpha/d\Omega)$ is the differential Raman cross section with units (cm^2 $molecule^{-1}$ sr^{-1}) and Γ_R is the Raman linewidth (Hz).

Combining (8) and (9), one obtains

$$I(\nu_{as})_{stim} = \frac{0.27d^2c^4\nu_{as}^2N_0^2}{n^4\sigma^2\nu_s{}^6\Gamma_R{}^2}(d\alpha/d\Omega)^2\ I(\nu_L)^2\ I(\nu_R) \qquad (10)$$

The intensity of the spontaneous Raman anti-Stoke's signal follows the expression

$$I(\nu_{as})_{spont} = \frac{N_1(d\alpha/d\Omega)I(\nu_L)d\Omega}{\sigma} \qquad (11)$$

Here $d\Omega$ is the fraction of Raman scattered light collected expressed in steradians. N_1, the population of v=1, can be obtained from the total Raman signal originating from v=0.

$$N_1 = 4\pi N_0(d\alpha/d\Omega)I(\nu_L)d \qquad (12)$$

Since the number of excited (v=1) states will build up with time (assuming slow VR), the spontaneous anti-Stoke's signal will build up

$$I(\nu_{as},t)_{spont} = \frac{4\pi N_0 d(d\alpha/d\Omega)^2\ I(\nu_L)^2\ d\Omega}{\sigma} \qquad (13)$$

For the purpose of estimating gain, the spontaneous anti-Stoke's signal will be taken after 1 sec excitation. Thus,

$$\text{gain} = \frac{I(\nu_{as})_{stim}}{I(\nu_{as})_{spont}} = \frac{(2.15 \times 10^{-2})N_0dc^4\nu_{as}^2I(\nu_R)}{n^4\sigma\nu_R{}^6\Gamma_R{}^2d\Omega} \qquad (14)$$

Assuming that the laser beam cross sections at the matrix are 2×10^{-3} cm^2, the matrix has a thickness of 0.05 cm, and the Raman linewidth[35] is 2×10^9 sec^{-1}, then the gain is found to be

$$g = 4.7 \times 10^{-14} I(\nu_R)$$

The dye laser can provide 7×10^{17} photons/sec at ν_R giving a final result

$$g = 3 \times 10^{4}$$

IX. Appendix II

An estimate for the upper limit to the VR time of N_2 in a dilute argon matrix can be obtained from our data and Equation (13).

The maximum power available from the argon laser at the matrix is 3.8 watts considering all reflection losses. This corresponds to a photon flux of 9×10^{18} photons/sec at 5145 Å. The differential Raman cross section for N_2 has been reported[16] as 5.4×10^{-31} cm^2 $molecule^{-1}$ sr^{-1} by Hyatt et al. In a matrix containing 1% N_2, the N_2 molecular density is approximately 2×10^{20} cm^{-3}. Taking the matrix thickness as 0.05 cm, the fraction of scattered light collected as 5.8×10^{-3} sr (spectrometer aperature), and the minimum laser beam cross section as 3×10^{-4} cm^2, the spontaneous Raman anti-Stoke's signal strength is

$$I(\nu_{as},t) = 5.7 \times 10^{-2} \text{ photons/sec per sec of irradiation}$$

Now if the VR time is at least a few minutes, the approximate signal strength after 2 minutes of excitation is 7 photons/sec since $N_1 << N_0$. This corresponds to a counting rate of about 50 counts/min considering the quantum efficiency of our photomultiplier. A signal this large should be extractable from a background of 200 counts/min if multiple scans are made. We were unable to confirm a signal of this magnitude so it does not seem probable that the VR time is longer than a few minutes.

X. References

1. H. Dubost, L. Abouaf-Marguin, and F. Legay, Phys. Rev. Lett. 29, 145 (1972).

2. L. J. Allamandola and J. W. Nibler, Chem. Phys. Lett. 28, 335 (1974).

3. D. S. Tinti and G. W. Robinson, J. Chem. Phys. 49, 3229 (1968).

4. H.-Y. Sun and S. A. Rice, J. Chem. Phys. 42, 3826 (1965).

5. D. J. Diestler, J. Chem. Phys. 60, 2692 (1974).

6. A. Nitzan and J. Jortner, Molec. Phys. 25, 713 (1973).

7. A. Nitzan, Shaul Mukamel, and J. Jortner, J. Chem. Phys. 60, 3929 (1974).

8. G. W. Robinson, J. Mol. Spectry. 6, 58 (1961).

9. G. J. Troup, "Photon Counting," Vol. 2, ed. J. H. Sanders and S. Stenholm (Pergamon Press, Oxford, 1974).

10. A. C. Albrecht, J. Chem. Phys. 34, 1476 (1961).

11. G. Herzberg, "Molecular Spectra and Molecular Structure. I. Spectra of Diatomic Molecules" (D. Van Nostrand, Inc., New York, 1950).

12. Calculated from vibrational constants reported by Tinti and Robinson in ref. 3.

13. J. E. Cahill and G. E. Leroi, J. Chem. Phys. 51, 1324 (1969).

14. A. Anderson, T. S. Sun, and M. C. A. Donkersloot, Canad. J. Phys. 48, 2265 (1970).

15. $\omega_e \approx 2351\ cm^{-1}$, $\omega_e x_e \approx 12\ cm^{-1}$.

16. H. A. Hyatt, J. M. Cherlow, W. R. Frenner, and S. P. S. Porto, J. Opt. Soc. Amer. 63, 1604 (1973).

17. Charlotte E. Moore, "Atomic Energy Levels, Vol. I," (U.S. Dept. Commerce, NBS, Circular 467), 1949.

18. A. Dienes, Opto-electronics 6, 99 (1974).

19. C. V. Shank and E. P. Ippen, Appl. Phys. Lett. 24, 373 (1974).

20. Frequency distribution functions for phonons in the rare gases have been obtained using neutron scattering techniques. Figures 21-23 show these functions for Ar, Ne, and Kr.

21. G. W. Robinson and R. P. Frosch, J. Chem. Phys. 38, 1187 (1963).

22. D. E. Stogryn and A. P. Stogryn, Molec. Phys. 11, 371 (1966).

23. J. M. Herbelin and G. Emanuel, "Air Force Report No. SAMSO-TR-74-15" (Space and Missile Systems Organization, Air Force Systems Command, Los Angeles Air Force Station, Los Angeles, California), Jan. 31, 1974.

24. D. C. Cartwright and T. H. Dunning, Jr., J. Physics B: Atom. Molec. Phys. 7, 1776 (1974).

25. M. F. Crawford, H. L. Welsh, and J. L. Locke, Phys. Rev. 75, 1607 (1949).

26. M. L. Oxholm and D. Williams, Phys. Rev. 76, 151 (1949).

27. E. Becker and G. Pimentel, J. Chem. Phys. 25, 224 (1956).

28. D. N. Batchelder, M. F. Collins, B. C. G. Haywood, and G. R. Sidney, J. Phys. C: Solid St. Phys. 3, 249 (1970).

29. J. S. Brown and G. K. Horton, Phys. Rev. Lett. 18, 647 (1967).

30. J. A. Leake, W. B. Daniels, J. Skalyo, B. C. Franzer, and G. Shirane, Phys. Rev. 181, 1251 (1969).

31. Although rotation is commonly neglected for molecules isolated in rare gas matrices at 4.2° K, it is possible that rotation of N_2 in solid argon is free or only slightly hindered. If this is indeed the case, then the unassigned lines in our Raman spectrum shown in Figure 3 may originate from upper rotational levels in the vibrational progression. Nitrogen has a small rotational constant (B_0 = 2.00 cm^{-1}) and if this gas phase value is used to roughly estimate the Boltzmann population of low-lying rotational levels in the ground vibrational state at 4.2° K, one finds that the population ratios of J=1 and J=2 compared to J=0 are 0.54 and 0.08 respectively.

Rotational Raman selection rules (see reference 10) allow transitions with $\Delta J=0, \pm 2$. Thus, the observed line at 2315.6 cm^{-1} may be the Raman transition $v=0$, $J=2 \rightarrow v=1$, $J=0$ which occurs at 2318.7 cm^{-1} in the gas phase while the line at 2310.6 cm^{-1} could be the transition $v=1$, $J=0 \rightarrow v=2$, $J=2$ (2313.7 cm^{-1} in the gas phase).

One might intuitively expect the population of v=0, J=2 to be larger than that of v=1, J=0 which would contradict the observed line intensities. However, if VR is indeed slow, one could expect the observed intensities.

These line assignments are highly tentative for at least two reasons. First, if rotation is occurring, it must be perturbed by the matrix to some extent. A complete rotational analysis would be required to see if rotational constants could be found consistent with the observed lines before these assignments could be confidently reported. Second, evidence of a barrier to rotation of 140 cm^{-1} (at 30° K) was

reported recently for CO in an argon matrix (see reference 32). CO has rotation and vibration constants similar to N_2 and a very small ($\approx$0.1 D) dipole moment. If these results are correct, it does not seem possible that rotation of N_2 in a solid argon matrix is completely unhindered.

32. G. J. Jiang, W. B. Person, and K. G. Brown, J. Chem. Phys. 62, 1201 (1975).

33. N. Bloembergen, Amer. J. Phys. 35, 989 (1967).

34. R. Begley, A. Harvey, and R. Byer, Appl. Phys. Lett. 25, 387 (1974).

35. J. B. Grun, A. K. McQuillan, and B. Stoicheff, Phys. Rev. 180, 61 (1969).